Preliminary geology of northern Hogem batholith, Quesnel terrane, north-central British Columbia

Luke Ootes[1, a], Anika Bergen[1], Dejan Milidragovic[1], Ben Graham[1], and Reid Simmonds[1]

[1] British Columbia Geological Survey, Ministry of Energy, Mines and Petroleum Resources, Victoria, BC, V8W 9N3
[a] corresponding author: Luke.Ootes@gov.bc.ca

Recommended citation: Ootes, L., Bergen, A., Milidragovic, D., Graham, B., and Simmonds, R., 2019. Preliminary geology of northern Hogem batholith, Quesnel terrane, north-central British Columbia. In: Geological Fieldwork 2018, British Columbia Ministry of Energy, Mines and Petroleum Resources, British Columbia Geological Survey Paper 2019-01, pp. 31-53.

Abstract

New bedrock mapping in parts of NTS 94C/04 (Notch Peak) and 93N/13 (Ogden Creek) refines the distribution and relationships of plutonic rocks in northern Hogem batholith. We recognize four plutonic suites (from oldest to youngest): Thane Creek, Duckling Creek, Mesilinka, and Osilinka. The ages of these suites are relative and are based on crosscutting relationships and the presence or absence of tectonic fabrics. The eastern part of the study area is mostly underlain by diorite and lesser hornblendite of the Thane Creek suite. The diorites consistently have a weak to strong foliation, with locally developed mylonite. Relatively potassic monzodiorite to quartz monzodiorite phases are common and may have resulted from late magmatic or secondary alteration processes. Foliated tonalite and granodiorite to quartz monzonite are also included with the Thane Creek suite, but lack of alteration and mylonite indicate they post-date the hornblendite and diorite intrusions. The southern part of the study area is underlain by Duckling Creek suite syenite and monzonite, with enclaves of pyroxenite (ca. 180 Ma). These rocks lack quartz, are rich in K-feldspar (commonly zoned) and display local magmatic layering, which is accentuated by deformation. The western part of the study area is underlain by foliated granites assigned to the Mesilinka suite (Jurassic to Cretaceous?). These granites commonly contain xenoliths of Thane Creek suite rocks, typically at higher elevations, some of which were foliated before incorporation into the granite. In the central part of the study area, the Osilinka suite granite is characterized by its low content of mafic minerals (≤5%). The granite lacks a foliation, but displays local evidence of post-crystallization ductile deformation. The youngest rocks in the study area are small (<4 m wide) subhorizontal sheets and lesser dikes of intermediate feldspar porphyry and felsic quartz-feldspar porphyry that cut the Osilinka granite. Previously documented metallic mineralization is recorded in ca. 34 MINFILE occurrences. During bedrock mapping, 17 new mineral occurrences were discovered. Most are within the Thane Creek and Duckling Creek suites and consist mainly of disseminated chalcopyrite and malachite staining. New gold and copper-bearing quartz veins were also discovered, and crosscut Thane Creek diorite and Osilinka granite.

Keywords: Hogem batholith, Quesnel terrane, Jurassic, Cretaceous, copper and gold

1. Introduction

In 2018, the British Columbia Geological Survey initiated a three-year mapping project in an area of north-central British Columbia (Fig. 1). The project aims to better understand the bedrock and surficial geology of the area, which includes rocks of the Quesnel, Stikine, and Cache Creek terranes (Figs. 1, 2) and metallic mineralization associated with these rocks (e.g., Lorraine Cu-Au porphyry deposit; Devine et al., 2014). This report presents the preliminary results of 1:50,000-scale bedrock mapping from the first field season, which focussed on mafic to felsic plutonic rocks of northern Hogem batholith and younger intrusive suites. A full-scale map is presented elsewhere (Ootes et al., 2019).

2. Setting and previous work

The 2018 study area (Figs. 2-4) includes part of northern Hogem batholith. The batholith is bounded to the north and east by volcanic and sedimentary rocks of the Takla Group (Triassic) along fault and intrusive contacts. To the west, Hogem batholith and Takla Group, both within Quesnel terrane, are juxtaposed against Cache Creek (Late Paleozoic to Triassic) and Stikine (Triassic to Jurassic) terranes across the Pinchi and Ingenika dextral strike-slip faults (Fig. 2).

The regional geology was originally mapped by Armstrong (1948), Lord (1949), and Armstrong and Roots (1948, 1954; also see Roots, 1954), who assigned rocks now included in Hogem batholith, to the 'Omineca intrusions' (Jurassic to Cretaceous). The local study area was mapped by Armstrong (1946) and Armstrong and Roots (1948, 1954). Although Roots (1954) gave thorough descriptions of a wide variety of intrusive units, he grouped these units as 'undivided' on his maps. Garnett (1972, 1978) subdivided southern Hogem batholith and Woodsworth (1976) subdivided northern Hogem batholith. Mapping by Ferri et al. (2001) in the northeast corner of 94C/04, and in areas to the east and north, focussed on the Takla Group and left the Hogem batholith largely undivided. In the south-central part of the study area, Nelson et al. (2003) updated mapping near the Hawk quartz vein-hosted gold prospect. Schiarizza and Tan (2005 a, b) mapped north of the 2018 study area; on their map, Schiarizza and Tan (2005b) plotted preliminary isotopic ages for plutonic rocks at the northern tip of Hogem batholith. Devine et al. (2014) studied

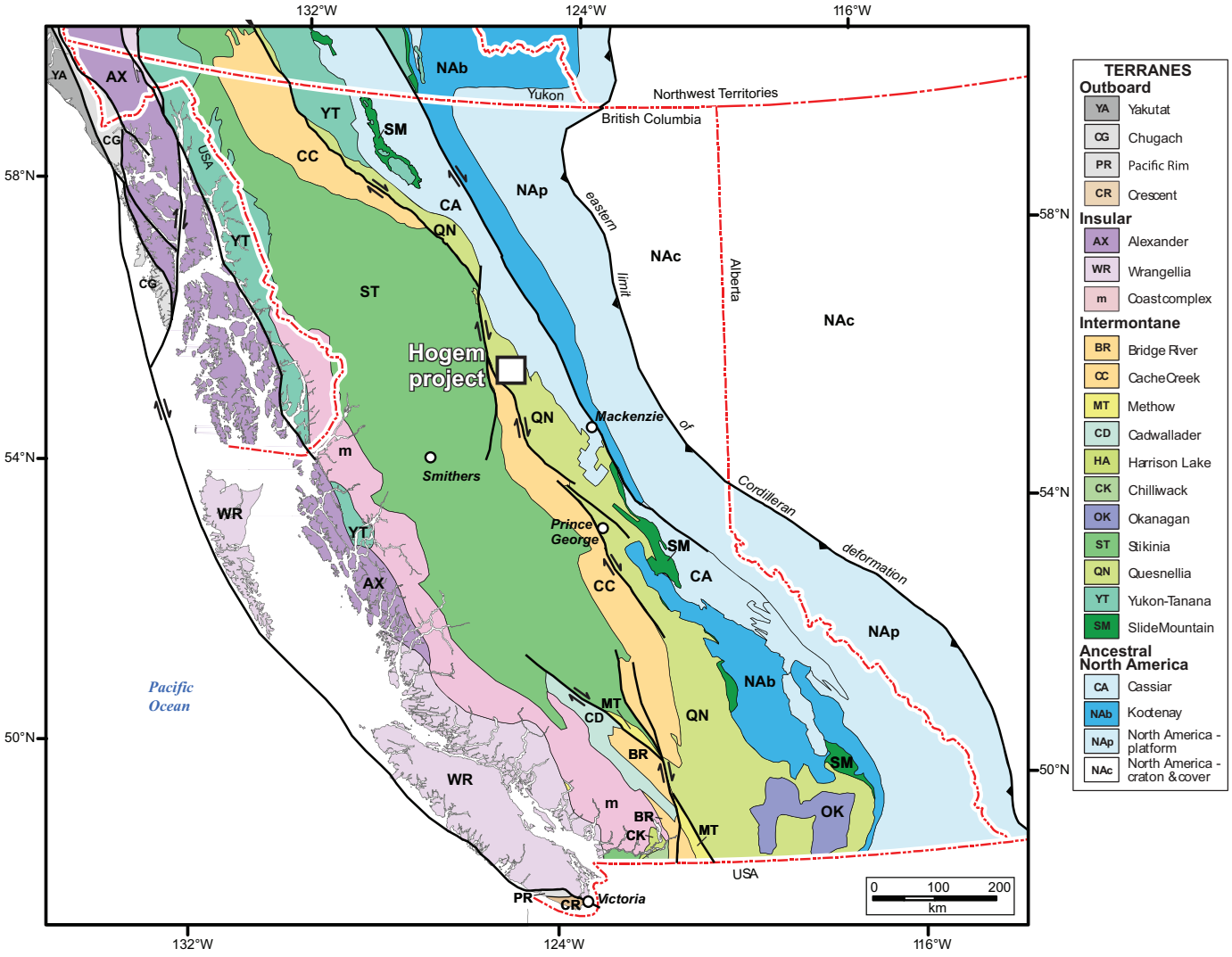

Fig. 1. Terrane map of British Columbia and neighbouring jurisdictions with location of study area. Modified after Nelson et al. (2013).

the Lorraine porphyry Cu-Au deposit, southeast of the 2018 map area and provided isotopic ages for the Duckling Creek suite. Recently, Madu and Ballantyne (2018) presented the results of an airborne geophysical survey flown with a line spacing of 250 m and a terrain-contouring elevation of 80 m. The survey included both radiometric (K, U, Th) and magnetic data collection (Fig. 3). Processed data and images of these data are available from GeoscienceBC (http://www.geosciencebc.com).

3. Bedrock geology

Mapping was conducted for two months in the summer of 2018 (Fig. 4; Ootes et al., 2019). Data were captured on tablets equipped with the Manifold (v.8.0) geographic information system, which also used georeferenced imagery, including aeromagnetic and radiometric maps from Madu and Ballantyne (2018). Each traversing pair carried a Terraplus KT-10 Magnetic Susceptibility Meter. About 10 discrete (non-scanning) measurements were acquired at each station (across an area up to 100 m^2) and the maximum, minimum, and mean were recorded (Fig. 5). Representative rock samples were collected and some prepared as polished thin sections (n=82). Thin section offcuts and a selection of other representative samples (n=65) were stained for K-feldspar. Results of samples collected for assay are presented below; geochemical and geochronological investigations are ongoing.

3.1. Lithologic units

The intrusive phases in northern Hogem batholith are organized into four suites (Fig. 4; Table 1), modified after Woodsworth (1976) and Woodsworth et al. (1991). The eastern and southwestern parts of the study area are underlain by diorite to monzodiorite and lesser hornblendite of the Thane Creek suite. In the west and southeast parts of the map area, the Thane Creek suite includes granodiorite, quartz monzodiorite, and tonalite. In the south-central part of the study area, the Duckling Creek suite comprises K-feldspar-rich syenite to monzonite. The Duckling Creek suite cuts the Thane Creek

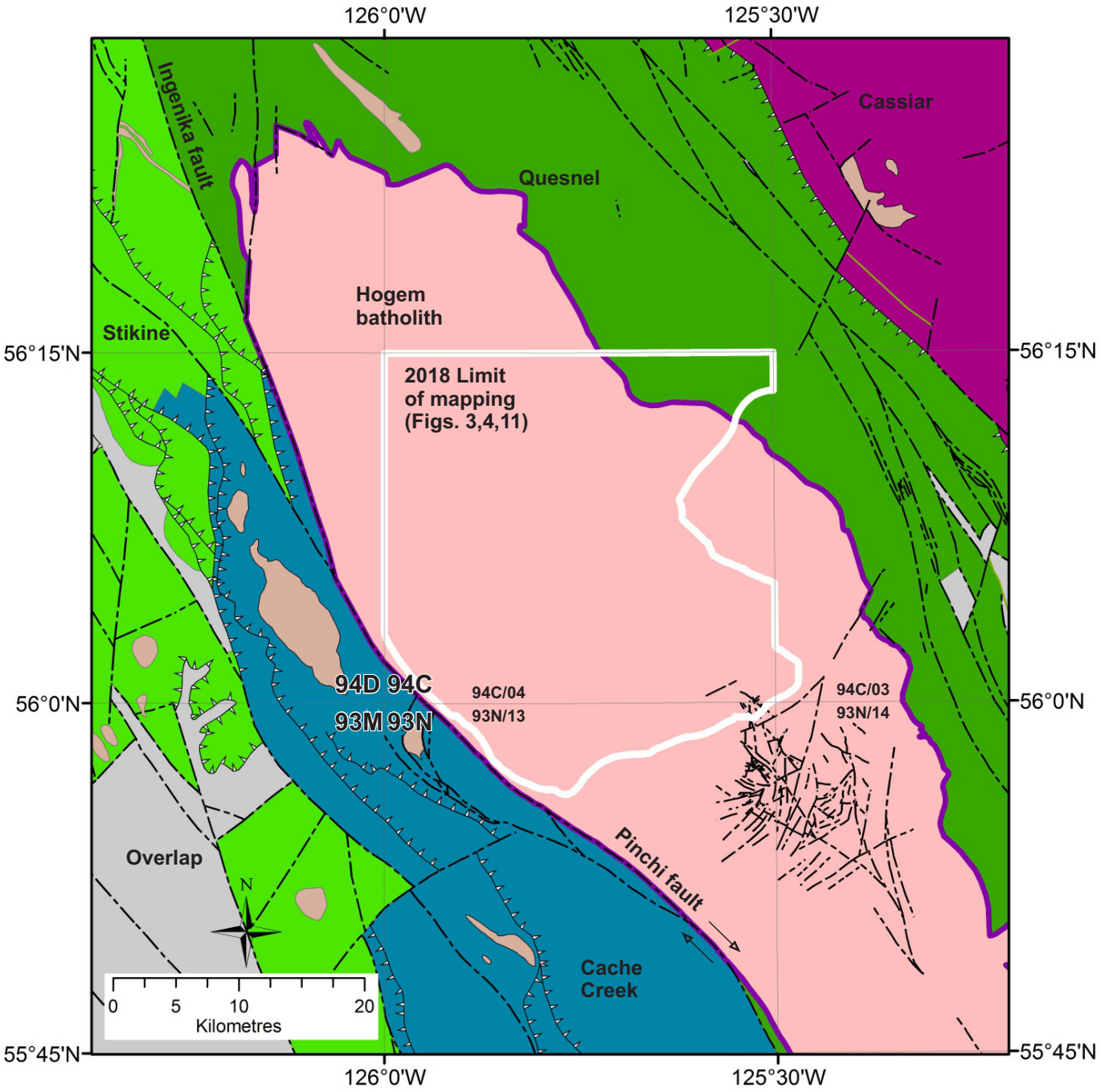

Fig. 2. Regional context of northern Hogem batholith and 2018 study area. Hogem batholith is in Quesnel terrane, which is separated from the Cache Creek and Stikine terranes by the Pinchi-Ingenika fault (dextral strike-slip). Thrust faults on the map have teeth on the hanging wall side; dashed lines are undifferentiated strike-slip and normal faults.

suite (Fig. 6). The western part of the study area is mainly underlain by Mesilinka suite granitic phases that cut the older Thane Creek suite (Fig. 6). In the central part of the study area is a unit of mafic-poor equigranular granite assigned to the Osilinka suite.

The only geochronological information directly from the study area is from K-Ar dating (Garnett, 1978; Woodsworth et al., 1991). Thus we rely on crosscutting relationships and the presence or absence of tectonic fabrics to establish relative ages of the suites. Uranium-lead zircon dates are available for selected units south and north of the study area (Fig. 6; Schiarizza and Tan, 2005b; Bath et al., 2014; Devine et al., 2014) and where appropriate these units are correlated to rocks in this study.

Table 1. Summary of plutonic map units, northern Hogem batholith.

Suite	Unit Code	Rock type and texture	Deformation	Relative magnetism	Other features	Mineralogy of note
Porphyry sheets		feldspar and quartz-feldspar porphyry	magmatic foliation (contact parallel)	low	fresh	
Osilinka	KHgg	equigranular granite	local shear zones	low	strongly jointed with local quartz veining	<5% biotite, altered to chlorite, local muscovite
Mesilinka	JHgg.or	K-feldspar porphyrytic granite	foliated	low, moderate when diorite xenoliths present	biotite foliation, local garnet and muscovite, abundant aplite and pegmatite dikes	allanite common
	JHgg.e	equigranular granite	foliated	low to moderate	K-feldspar phenocrysts up to 5 cm	allanite common
Duckling Creek	JHds	syenite to monzonite	magmatic layering and foliated	high	K-feldspar rich and quartz deficient, magmatic layering, zoned K-feldspar, and K-feldspar pegmatite common	sodic(?) amphibole and pyroxene, apatite and titanite common
	JHds	pyroxenite	magmatic layering and foliated	high to highest	Malachite staining common	contains biotite
Thane Creek	JHgt	tonalite	foliated	low	grey, lacks K-felspar, foliated	mostly plagioclase and quartz
	JHgd	granodiorite to quartz monzonite	foliated	moderate to high	contains quartz, variable amounts of biotite, and does not appear altered	pristine igneous mineralogy, magnetite and titanite common
	JHdd	diorite to quartz monzodiorite	foliated to locally mylonitic	low to high	equigranular hornblende-plagioclase bearing; locally moderately to extensively altered and locally strongly deformed, some malachite staining	extensive biotite and epidote, and little amphibole, coincide with K-feldspar-bearing phases, titanite, apatite, and magnetite common
	JHuhb	hornblendite	foliated	high to highest	black coarse-grained to pegmatitic; locally mingled with diorite, some malachite staining and disseminated chalcopyrite	coarse amphibole is overgrown by secondary amphibole and biotite, titanite, magnetite, and chalcopyrite common

3.1.1. Thane Creek suite

3.1.1.1. Hornblendite

Black to salt and pepper, medium-grained to pegmatitic hornblendite forms ≤100 m wide plutons (unit JHuhb) scattered through the diorite phases of the Thane Creek suite (Figs. 4-7; Table 1). Dark green amphibole crystals, with rare corroded clinopyroxene cores, predominate, and range from medium to coarse grained. Plagioclase, where present, is interstitial between amphibole and ranges from fine to coarse grained (Fig. 7a). Biotite, generally medium grained, is common in the hornblendites, in concentrations ranging from 0 to 20%. Accessory euhedral titanite and euhedral to subhedral crystals of apatite are also common. Magnetite abundance in hornblendite varies (mostly ≤5%), and these rocks have a strong magnetic signature (Fig. 5). Epidote is a secondary alteration phase in the hornblendite, and is generally ≤5% of the rock. Trace amounts of disseminated pyrite and chalcopyrite occur and, in a few small outcrops (~1 m^2), chalcopyrite comprises a few percent of the rock. Some of the sulphide-bearing rocks have local malachite or iron rust staining on weathered surfaces. The hornblendites are entirely within diorite (Fig. 4) and display both sharp and diffuse contacts, the latter indicating magma co-mingling (Fig. 7b). We interpret that the hornblendites are comagmatic with the diorite plutons and that they either represent crystal cumulates formed from a more primitive parental magma, or injections of a hydrous mafic to ultramafic magma into a predominantly dioritic chamber.

3.1.1.2. Diorite to quartz monzodiorite

The eastern and southwestern parts of the study area are mostly underlain by green and white to black and white weathering, equigranular, medium- to coarse-grained diorite that is foliated to locally mylonitic (unit JHdd; Figs. 4-7). The diorite (Fig. 7c) consists mostly of plagioclase and hornblende, but locally transitions to units with more significant amounts of quartz and K-feldspar (quartz diorite, quartz monzodiorite, monzodiorite) and potentially gabbro. Accessory phases include clinopyroxene (as corroded cores to amphibole), euhedral to subhedral titanite, magnetite, and apatite. Epidote is locally common and interpreted as an alteration product

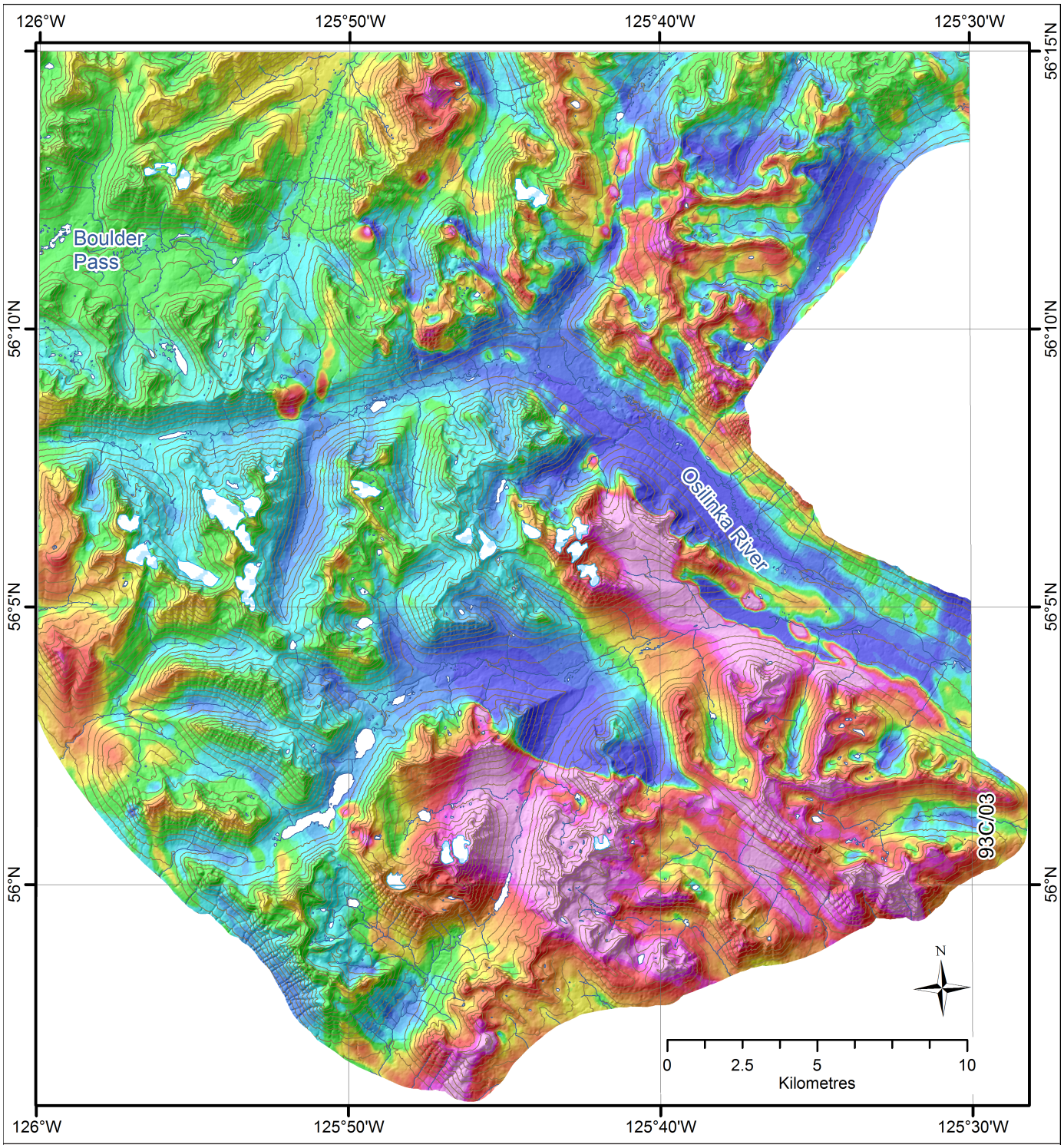

Fig. 3. a) Magnetic map of 2018 study area; warm colours (pink-white) correspond to high magnetism and cool colours (blue) correspond to low magnetism. From Madu and Ballantyne (2018).

(Table 1). The diorite locally contains biotite, in some cases in much greater abundance than amphibole, but it has not been resolved if the biotite is a primary magmatic or secondary metamorphic/alteration phase. The relatively potassic phases contain blotchy pink K-feldspar in the groundmass, which is locally accompanied by mint-green weathering (Fig. 7d). These zones correspond to biotite- and epidote-rich phases, where plagioclase has been altered to clay minerals, amphibole is rare, and titanite locally displays highly corroded grain boundaries. These features may indicate either late magmatic or secondary potassic alteration. Although our preliminarily interpretation favours secondary alteration for many potassic

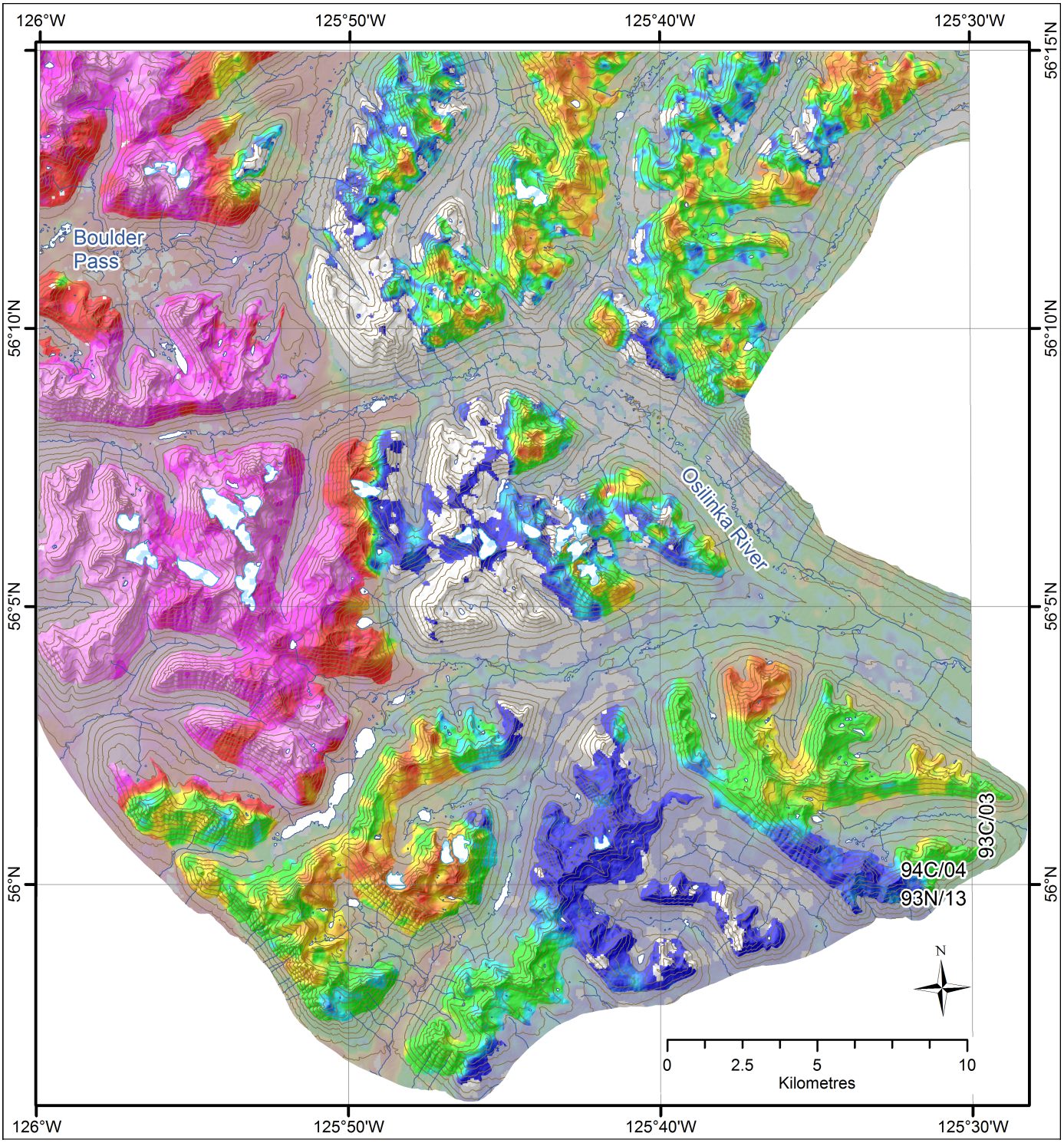

Fig. 3. b) Th/K map of 2018 study area; warm colours correspond to high Th/K and cool colours correspond to low Th/K. White zones are areas of no data. Grey overlay mask represents surficial cover. Draped on shaded relief map, contour intervals are 100 m. From Madu and Ballantyne (2018).

units, true magmatic monzodiorite may also be present. The diorite contains variable abundances of magnetite; this variation could be from magmatic fractionation, secondary alteration, or both. The magnetic variation is evident from magnetic susceptibility measurements (Fig. 5), which correlate with magnetic variations on airborne magnetic maps (Fig. 3a). Phase transitions from diorite to monzodiorite coincide with the variation of K on the radiometric maps (Fig. 3b).

The diorite crosscuts and comingles with the hornblendite (Fig. 7b). Where there is comingling (Fig. 7b), the rocks are texturally and compositionally heterogeneous in terms of amphibole, plagioclase, and magnetite concentrations. In

some locations, the combined effects of mixing with enclaves, magmatic differentiation, and K-alteration, resulted in textural and compositional variations of a scale too small to map. The diorite locally contains xenoliths of layered fine-grained green rock, possibly derived from the Takla Group. The diorite is locally stained with malachite and rarely contains disseminated chalcopyrite (<1%).

Near its western margin, diorite is cut by Mesilinka suite equigranular granite and K-feldspar porphyritic granite (Fig. 4; Woodsworth, 1976). In the central part of the map area, diorite and, at one outcrop, hornblendite, are in sharp contact with crosscutting Osilinka suite equigranular granite (Fig. 4); rare xenoliths of diorite are in the granite.

Devine et al. (2014) described the Rhonda-Dorothy gabbro-diorite body, about 20 kilometres south of the study area, and documented a U-Pb zircon crystallization age of 200.9 ±0.2 Ma. Based on descriptions in Devine et al. (2014) we suggest that the Thane Creek and Rhonda-Dorothy bodies are equivalent. The Thane Creek diorite may be also be equivalent to diorite plutons that cut the Takla Group north of the Hogem batholith, for which Schiarizza and Tan (2005b) gave preliminary ages of 224 to 211 Ma. We tentatively regard the age of the Thane Creek diorite as ca. 200 Ma (Fig. 6).

3.1.1.3. Tonalite

Tonalite (unit JHgt) outcrops in three areas near the western boundary of the study area (Figs. 4-7). It is equigranular, medium-grained, white to grey, with a moderate foliation. Quartz and plagioclase are accompanied by biotite, and accessory allanite. The rocks lack amphibole, K-feldspar, titanite, and magnetite (Table 1). In the northwest, tonalite is crosscut by fine-grained equigranular granite dikes and sheets that commonly contain garnet (Fig. 7e). Farther east, the tonalite is cut by granitic rocks of the Mesilinka suite (Figs. 4, 6). Tonalite xenoliths in the granites can contain secondary muscovite. The tonalite has a low to moderate magnetic signature (Fig. 5) and airborne radiometrics indicate low K, and moderate to high Th-U. The tonalite is interpreted to be younger than the Thane Creek diorite (Fig. 6) because the tonalite lacks alteration and, although foliated, it lacks strong deformation features such as mylonite. North of Hogem batholith, Schiarizza and Tan (2005b) mapped a tonalite body that cuts the Takla Group and gave a preliminary age estimate of ca. 174 Ma.

3.1.1.4. Granodiorite to quartz monzonite

A unit that ranges from granodiorite to quartz monzodiorite to quartz monzonite (unit JHgd) outcrops in the northwest, southwest, and southeast parts of the study area (Fig. 4). These rocks are equigranular to weakly plagioclase porphyritic, and medium grained (Fig. 7f). They contain quartz (10-25%), weakly kinked biotite, which is locally more abundant than amphibole, and K-feldspar (20-30%) with well-developed crystal habit. Primary accessory phases include euhedral titanite and magnetite. Subrounded fine- to medium-grained xenoliths of intermediate composition are common (Fig. 7f). This unit has a moderate to strong magnetic expression (Fig. 5) and has Th>K>U (Fig. 3b).

These rocks are interpreted to be younger than the Thane Creek diorite (Fig. 6) because they lack hornblendite phases, potassic alteration, and strong deformation. This unit may be older than the Duckling Creek suite because it is locally cut by K-feldspar pegmatites, but other intrusive contacts have not been observed. In the southwest part of the study area, this unit forms outcrops near tonalite (Fig. 4), but intrusive relationships were not observed and their temporal relationships are unresolved (Fig. 6).

3.1.2. Duckling Creek suite

The south-southeast part of the study area is underlain by quartz-free, K-feldspar-rich rocks of the Duckling Creek suite (unit JHds; Figs. 4, 8), previously referred to as the Duckling Creek Syenite Complex (Woodsworth, 1976; Garnett, 1978; Nixon and Peatfield, 2003; Devine et al., 2014). The Duckling Creek suite is mostly syenite to monzonite, with lesser monzodiorite and local zones of biotite pyroxenite. These rocks are texturally heterogeneous (Fig. 8), ranging from equigranular to porphyritic to pegmatitic. Porphyrytic varieties contain K-feldspar phenocrysts (commonly zoned) in a groundmass of equigranular green amphibole and lesser plagioclase (possibly albite). They contain accessory subhedral to euhedral titanite and apatite, and variable amounts of magnetite with a subhedral to interstitial habit within amphibole-rich, polycrystalline aggregates. Rhythmic magmatic layering is common, with aligned K-feldspar phenocrysts that are further accentuated by deformation (Fig. 8c). Local pyroxenite enclaves, with dimensions in the scale of 10s of metres, are exposed mostly at higher elevations, where they are intruded by the more intermediate to felsic phases (Fig. 8a). The entire unit has moderate to strong magnetism (Fig. 5), with areas of highest magnetism spatially associated with exposed biotite pyroxenite. On the airborne radiometric map, the Duckling Creek suite has low Th/K (Fig. 3b), reflecting its K-rich character. The biotite pyroxenite zones are commonly stained with malachite and locally contain disseminated chalcopyrite.

South of the study area, Devine et al. (2014) identified three stages of the Duckling Creek suite and constrained their timing with U-Pb zircon ages: 1) biotite pyroxenite (ca. 182 to 178.5 Ma), which can contain base- and precious-metal mineralization and associated alteration (e.g., Lorraine Cu-Au deposit); 2) predominantly K-feldspar porphyritic syenite to monzonite (ca. 178.8 to 178.4 Ma); and 3) massive syenite and pegmatite (ca. 177 to 175 Ma). The older biotite pyroxenite (Fig. 7a) locally contains malachite staining and disseminated chalcopyrite and likely corresponds with Devine et al. (2014) stage 1. The more typical syenite to monzonite (Fig. 8) corresponds with Devine et al. (2014) stage 2.

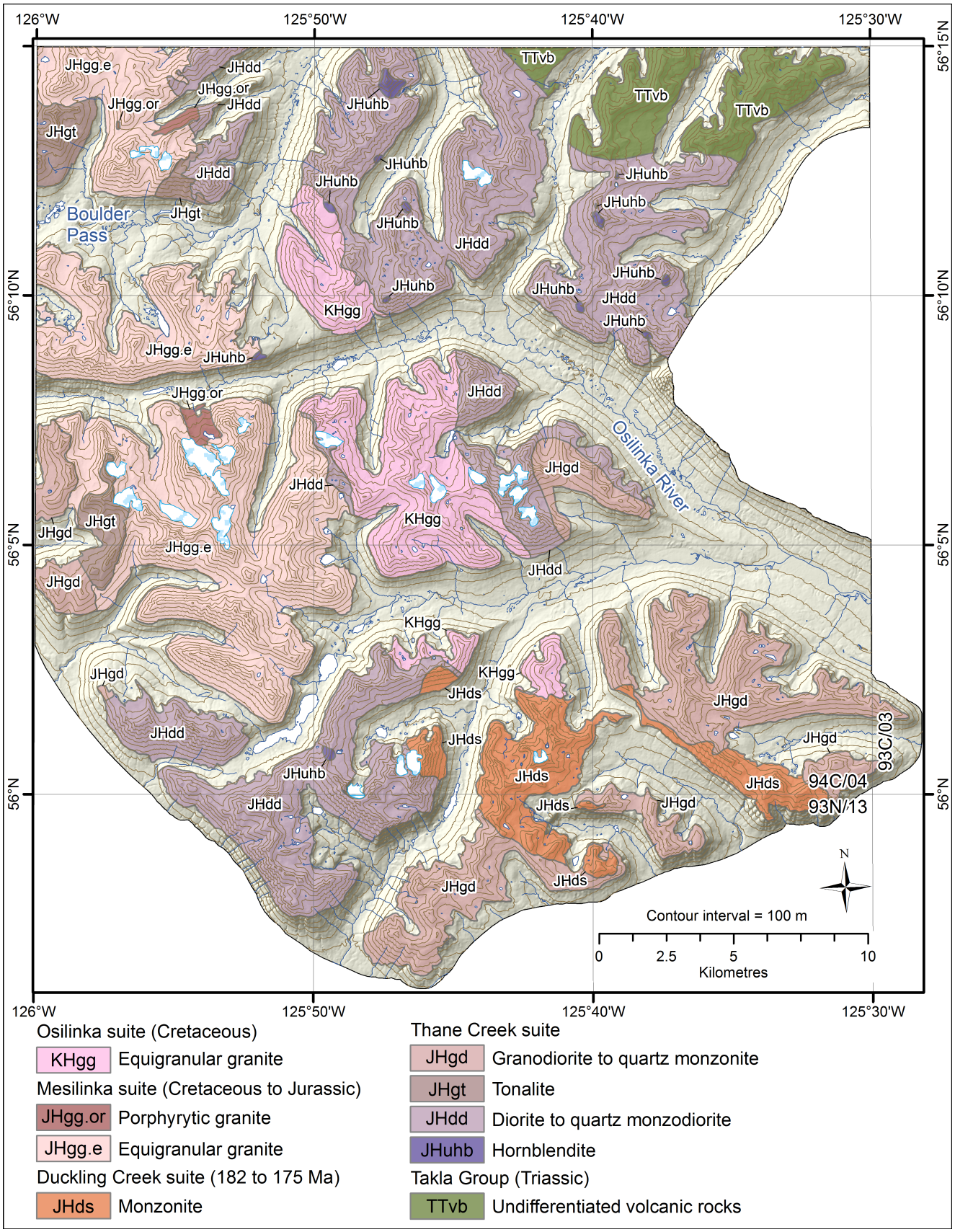

Fig. 4. a) Geology of northern Hogem batholith, generalized from Ootes et al. (2019). Intrusive suite names are modified from Woodsworth (1976). The Takla Group is from Ferri et al. (2001).

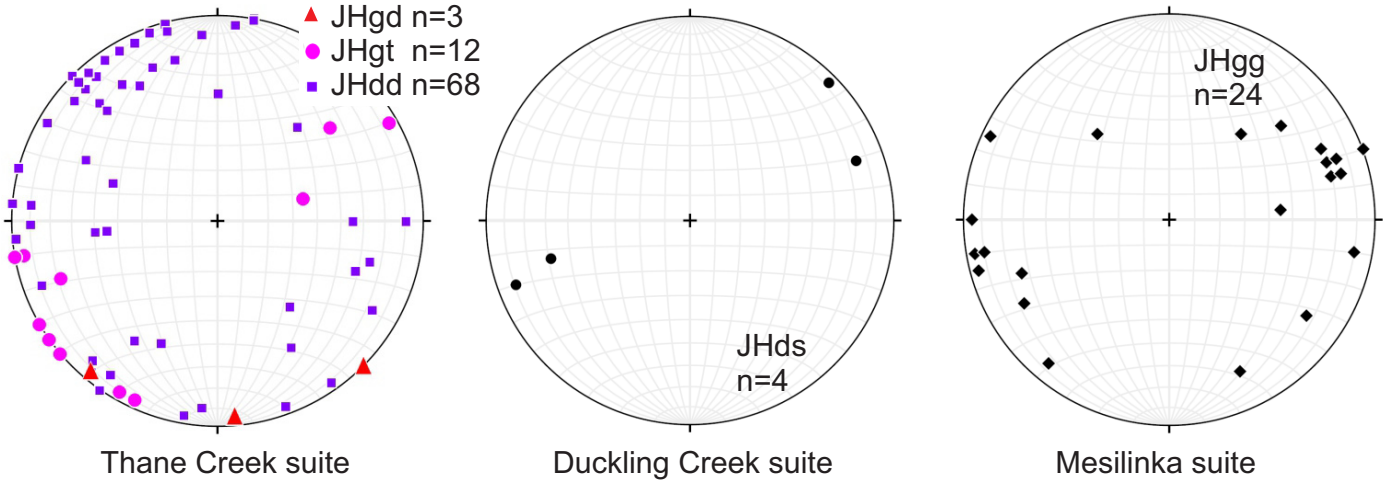

Fig. 4. b) Equal area lower hemisphere projections of poles to foliation planes for Thane Creek suite diorite (blue squares), tonalite (pink circles), and granodiorite (pink triangles), Duckling Creek suite rocks, and Mesilinka suite granites. Plots generated using Allmendinger software, available at http://www.geo.cornell.edu/geology/faculty/RWA/programs/stereonet.html.

3.1.3. Mesilinka suite

3.1.3.1. Equigranular granite

Throughout the western part of the study area the predominant rock type is equigranular granite (unit JHgg.e; Figs. 4, 9a). The granite is medium grained, light pink to grey, and contains biotite (10-20%) that is kinked. Accessory phases include allanite, apatite, and zircon (Table 1). This granite contains a foliation defined by aligned biotite, which helps distinguish it from equigranular granite of the younger, biotite-deficient Osilinka suite (Fig. 4). The equigranular granite contains xenoliths of tonalite, which locally contain muscovite. Close to the xenoliths the granite contains garnet (Fig. 9a).

At higher elevations to the southwest (Fig. 4), the granite contains xenoliths of Thane Creek suite diorite, and has a relatively high magnetic expression. At lower elevations the granite is xenolith-free and has a low magnetic expression. The elevation-related appearance of diorite xenoliths may indicate that these are roof pendants, possibly indicating proximity to the top of the original magma chamber, whereas lower elevations represent the main granite body. We note that the magnetic signature in some areas appears to be topographically controlled, evident when the magnetic map is draped on elevation datum (Fig. 3a). This is best explained by erosion having variably incised this granitic body, leaving higher magnetic expressions that coincide with diorite xenoliths at higher elevations.

3.1.3.2. Porphyritic granite

The youngest mappable Mesilinka phase is porphyritic granite with K-feldspar phenocrysts (≤5 cm long) in a medium- to coarse-grained equigranular groundmass (unit JHgg.or; Figs. 4 and 9b). The granite contains biotite, with accessory apatite, magnetite, allanite, and zircon (Table 1). It cuts the equigranular granite, and Thane Creek suite tonalite and diorite (Figs. 4, 6). The granite displays a foliation defined by aligned feldspar phenocrysts and biotite and this fabric crosscuts the intrusive contacts (Fig. 9c). The porphyritic granite has a low to medium aeromagnetic expression (Fig. 5). Both this unit and the equigranular granite have a high Th expression on airborne radiometric map, with Th >K (Fig. 3b). North of the study area, Schiarizza and Tan (2005b) reported a preliminary U-Pb zircon age of ca. 135 Ma from a Mesilinka granite.

3.1.4. Osilinka suite

The central part of the study area is underlain by equigranular granite (unit KHgg; Figs. 4, 10). Woodsworth (1976) mapped this unit as one of several 'massive granodiorite plutons' that he considered the youngest mappable units in northern Hogem batholith. These plutons were subsequently referred to as the Osilinka stocks by Woodsworth et al. (1991) and the Osilinka pluton by Nelson et al. (2003). The granite is medium grained and white, with a low mafic mineral content (<5%; Fig. 10). Plagioclase displays strong oscillatory zoning, and both feldspars typically have extensively corroded cores. This and the lack of a foliation distinguishes it from the biotite-bearing, foliated equigranular granite of the Mesilinka suite (Fig. 4). Compared to other intrusive suites in northern Hogem batholith, the granite is distinctinctly jointed. Some joints contain quartz veins and associated alteration haloes (locally muscovite-bearing) in the adjacent granite. The Osilinka suite mainly cuts the Thane Creek suite diorite but, in the southeast, it cuts Duckling Creek suite syenite. Along its western margin, the granite intruded the Mesilinka suite (Figs. 4, 6). The granite has a low magnetic expression and is characterized by K >Th (Figs. 3, 5). Schiarizza and Tan (2005b) reported a U-Pb titanite date of 134.0 ±1.2 Ma for an Osilinka stock at the north end of Hogem batholith, and a U-Pb zircon age of 136.6 ±0.7 Ma for a small stock north of the batholith.

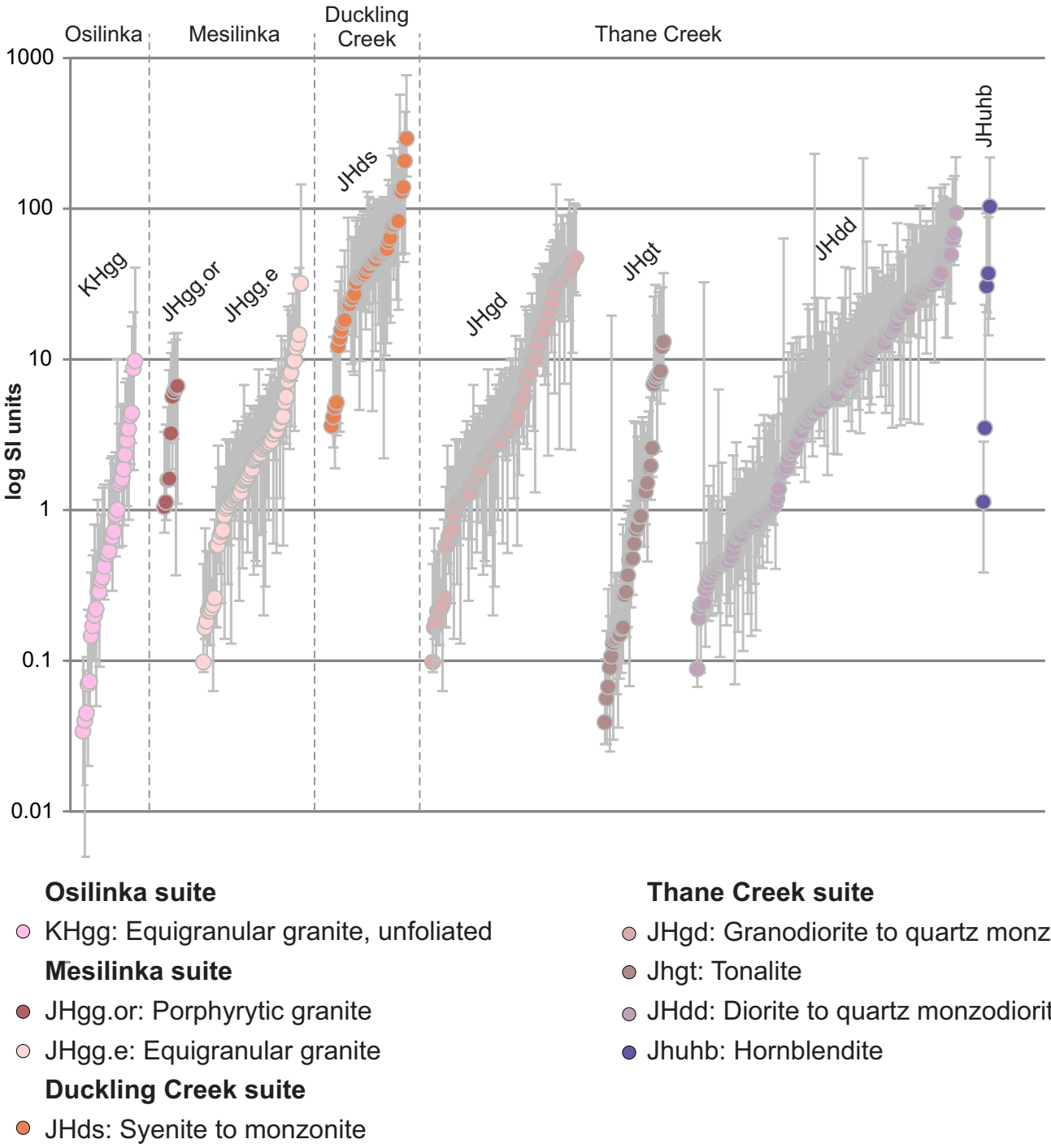

Fig. 5. Plot of magnetic susceptibility (logSI: International System of Units) for each of the intrusive suites. Each point represents the mean of ca. 10 measurements that were collected at each field station. Error bars represent the maximum and minimum measurements associated with each mean.

3.1.5. Porphyry sheets and dikes

Subhorizontal sheets and rare dikes of feldspar porphyry and quartz-feldspar porphyry cut equigranular granite of the Osilinka suite (Figs. 10c, d). The sheets are the youngest rock unit identified in the study area. They are <4 m wide and include at least two different subtypes characterized by: 1) plagioclase phenocrysts (≤4 cm) in a brown to dark green fine-grained intermediate groundmass; and 2) quartz (≤1 cm) and K-feldspar phenocrysts (≤2 cm; Fig. 10c), commonly densely packed, in a fine-grained white to light green felsic groundmass. Upper and lower contacts with the equigranular granite are common and are generally chilled and sheared. The sheets lack the jointing that is common in the equigranular granite.

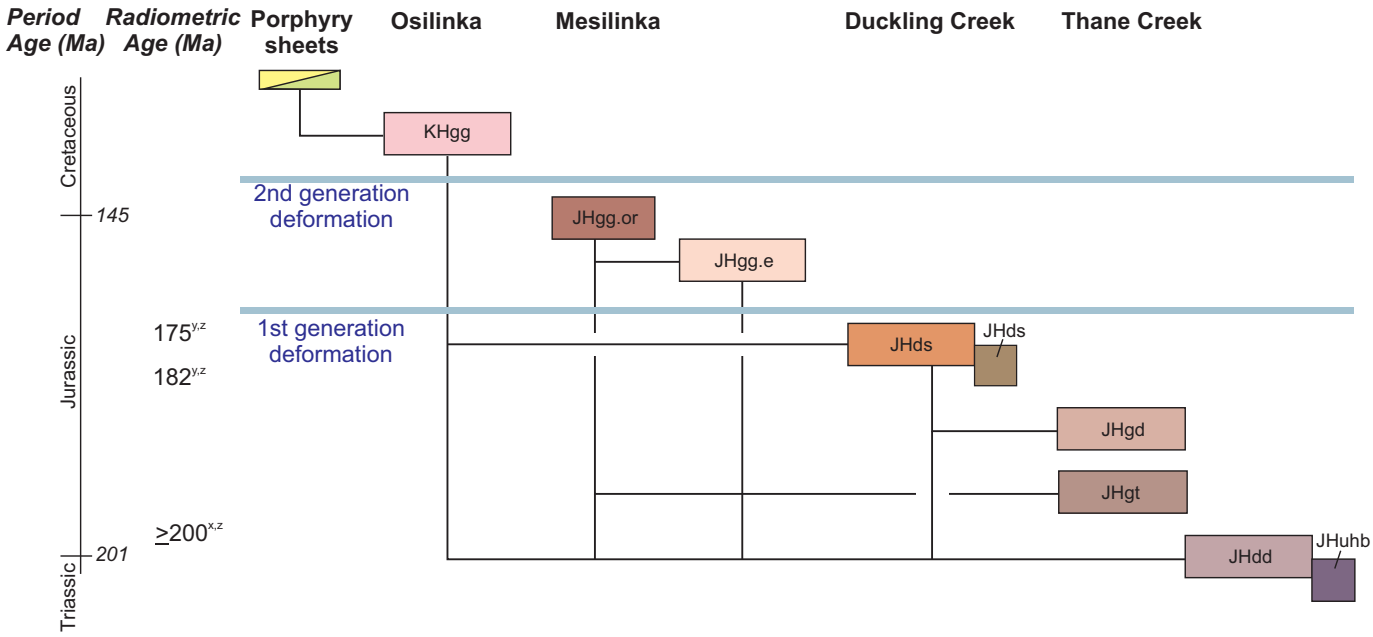

Fig. 6. Flow chart depicting the intrusive (thin black lines) and structural (thick blue lines) relationships of plutonic rocks in northern Hogem batholith. Observed crosscutting relationships are depicted by lines that connect units. Radiometric age data are from [x]Schiarizza and Tan (2005b), [y]Bath et al. (2014), and [z]Devine et al. (2014).

3.2. Structural observations

The diorite to quartz monzodiorite of the Thane Creek suite contains a weak to strong foliation (Fig. 4b), including local mylonite. The foliation is defined by the amphibole, plagioclase, and biotite. Within the diorite, flattened and aligned hornblendite enclaves and amphibole-biotite schlieren are primary magmatic features that were overprinted and accentuated by tectonic deformation. The hornblendite units do not contain a foliation, indicating that these bodies were likely more rigid than surrounding diorite during deformation, possibly due to coarse grain sizes. The tonalite and granodiorite to quartz monzodiorite units of the Thane Creek suite contain a weak to moderate foliation, typically defined by biotite and amphibole. The relationship of this fabric to the foliation in the diorite is unknown.

Syenite and monzonite of the Duckling Creek suite are weakly to strongly foliated (Fig. 4b), including local mylonite development. Similar fabrics are described from the oldest unit of the suite, south of the study area (Devine et al., 2014). The foliation is defined by coarse-grained K-feldspar with microlithons of medium-grained amphibole and lesser pyroxene and plagioclase or albite. Typically, the finer-grained mafic units appear more strongly deformed than the coarser-grained amphibole-poor rocks. Magmatic layering, in places rhythmic and graded, is a common feature in the monzonite and is interpreted to be a result of primary magmatic differentiation accentuated by ductile deformation (Fig. 8c).

Both porphyritic granite and equigranular granite of the Mesilinka suite have a moderate tectonic foliation (Fig. 4b), which cuts across intrusive contacts (Fig. 9c). In the northwest part of the study area, near the contact between the porphyritic granite and Thane Creek diorite and where outcrops are inaccessible, is talus with strongly deformed to mylonitic diorite. In the south-central part of the study area, the foliated equigranular granite contains xenoliths of diorite with an earlier formed, moderate to strong foliation, including local mylonite. Based on these observations, it appears that the Thane Creek diorite was deformed before, or possibly during, intrusion of the Mesilinka granite.

The Osilinka suite equigranular granite lacks a foliation, but does preserve evidence of post-crystallization ductile deformation. This evidence is, in part, within a two metre-wide intermediate dike that crosscuts the granite in the central part of the Osilinka suite (Fig. 4a). The granite lacks a fabric, whereas the dike contains a strong north striking foliation, and moderately north-plunging mineral lineations and boudins, and symmetric winged porphyroclasts. The relationship of this dike and porphyry dikes is unknown. Ductile deformation is also indicated by a weakly developed foliation in ≤20 cm wide alteration haloes adjacent to joints and quartz veins in the central part of the Osilinka suite. These alteration haloes likely resulted from fluid-rock interaction during quartz vein formation. The foliation in these haloes is perpendicular to the joints and veins and is gently folded, but the timing relationship between the joints and quartz vein and the foliation is unknown. These structures may be local, or may be the manifestation of regional deformation, with the paucity of mafic minerals accounting for the absence of a foliation in the granite itself.

The quartz-feldspar and feldspar porphyry sheets contain a contact-parallel foliation. This fabric is interpreted to be magmatic because it does not crosscut contacts, it does not occur in the equigranular granite, and it only developed close

Fig. 7. Representative outcrop photographs of Thane Creek suite. **a)** Coarse-grained hornblendite (Jhuhb) with pegmatitic phase of amphibole and plagioclase. **b)** Diffuse intrusive contact between hornblendite (dark) and diorite (green-grey). **c)** Equigranular, medium-grained diorite (Jhdd). **d)** Monzodiorite with subhedral pink K-feldspar crystals and mint green epidote-bearing groundmass. Mafic crystals retain the shape of amphibole but are mostly replaced by biotite, which is interpreted to record late- or post-magmatic potassic alteration. **e)** Tonalite (JHgt), crosscut by subhorizontal aplite sheet and older aplite dikelets. **f)** Equigranular quartz monzodiorite to granodiorite (JHgd) with subrounded intermediate xenoliths.

to the margins of the sheets, not in the cores. The fabrics that occur in the equigranular granite were not observed in the porphyry sheets.

4. Mineralization

The Lorraine Cu-Au porphyry deposit is 11 km southeast of this study and is hosted in rocks of the Duckling Creek suite (Garnett, 1978; Nixon and Peatfield, 2003; Bath et al., 2014,; Devine et al., 2014). There are no developed prospects within the study area, but ca. 34 mineral occurrences are documented in MINFILE (Fig. 11; Table 2). These can be considered as two end-member styles of mineralization. First, syngenetic

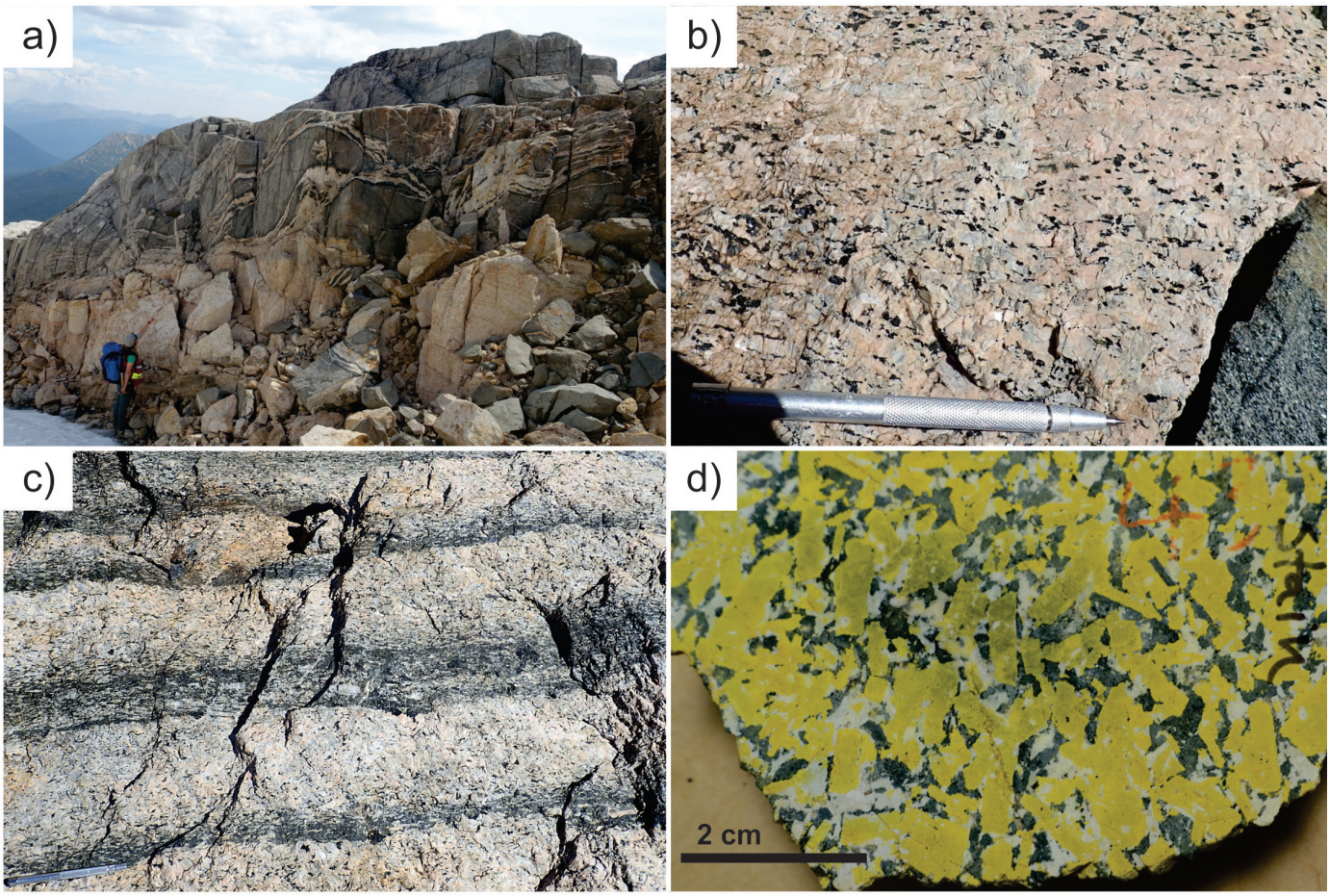

Fig. 8. Representative outcrop photographs of the Duckling Creek suite. **a)** Large pyroxenite enclaves in syenite. **b)** Coarse-grained syenite with K-feldspar and amphibole. **c)** Rhythmic magmatic layering that ranges from monzodiorite to syenite in composition. The layering is accentuated by a foliation, defined by alignment of the K-feldspar subparallel to the layers. **d)** Stained slab of monzonite showing coarse K-feldspar (yellow) and interstitial albite or plagioclase (white) and amphibole or pyroxene (black).

porphyry-style Cu (±Au, Ag, Mo; Fig. 11; Table 2), which is typically represented by malachite staining or disseminated chalcopyrite in the host rock. Most mineral showings of this type are in diorite and granodiorite of the Thane Creek suite and pyroxenite of the Duckling Creek suite, although one Mo-showing is related to the Osilinka granite (Fig. 11; Table 2). The second style includes epigenetic quartz veins with local concentrations of precious- and base-metals (Fig. 11; Table 2) that are relatively young as they cut the Osilinka granite (e.g., Hawk showing; Nelson et al., 2001).

While mapping, we collected grab samples with metallic mineralization from outcrops. These samples were sent to Activation Laboratories (Ancaster, Ontario) where they were crushed and pulped using mild steel (Code RX-1) and analyzed by a combination of instrumental neutron activation analysis (INAA) and acid dilution inductively coupled plasma-mass spectrometry (ICP-MS; Code 1H; Table 3). Two samples contained Cu values above detection limit of 10,000 ppm and were further analyzed by acid dilution inductively coupled plasma optical emission spectrometry (ICP-OES; Table 3).

The results document 17 new mineral occurrences, two of which are close to previously documented mineralization (Fig. 11; Tables 2 and 3). These occurrences conform to the same two end-member styles described above. Most are of the porphyry-style and comprise malachite staining and/or disseminated chalcopyrite. At location B (Fig. 11; Table 3) chalcopyrite occurs in veins and as disseminations in hornblendite of the Thane Creek suite, but most others are in Thane Creek diorite or granodiorite, or in pyroxenite of the Duckling Creek suite. The latter includes location L (Fig. 11; Table 3), which has malachite staining on a magnetite-cemented breccia zone in pyroxenite. Two of the new mineral occurrences are quartz vein-hosted. At location C (Fig. 11) mineralization is in a quartz vein (up to 15 cm wide) that pinches and swells, is exposed intermittently over ~100 m, and locally displays a malachite stain and disseminated chalcopyrite. At location E (Fig. 11) mineralization is in a poorly exposed subhorizontal 10 cm-wide quartz vein. Where exposed and in talus the quartz vein contains massive and disseminated pyrite, and carries minor amounts of Au, and elevated Mo (Table 3).

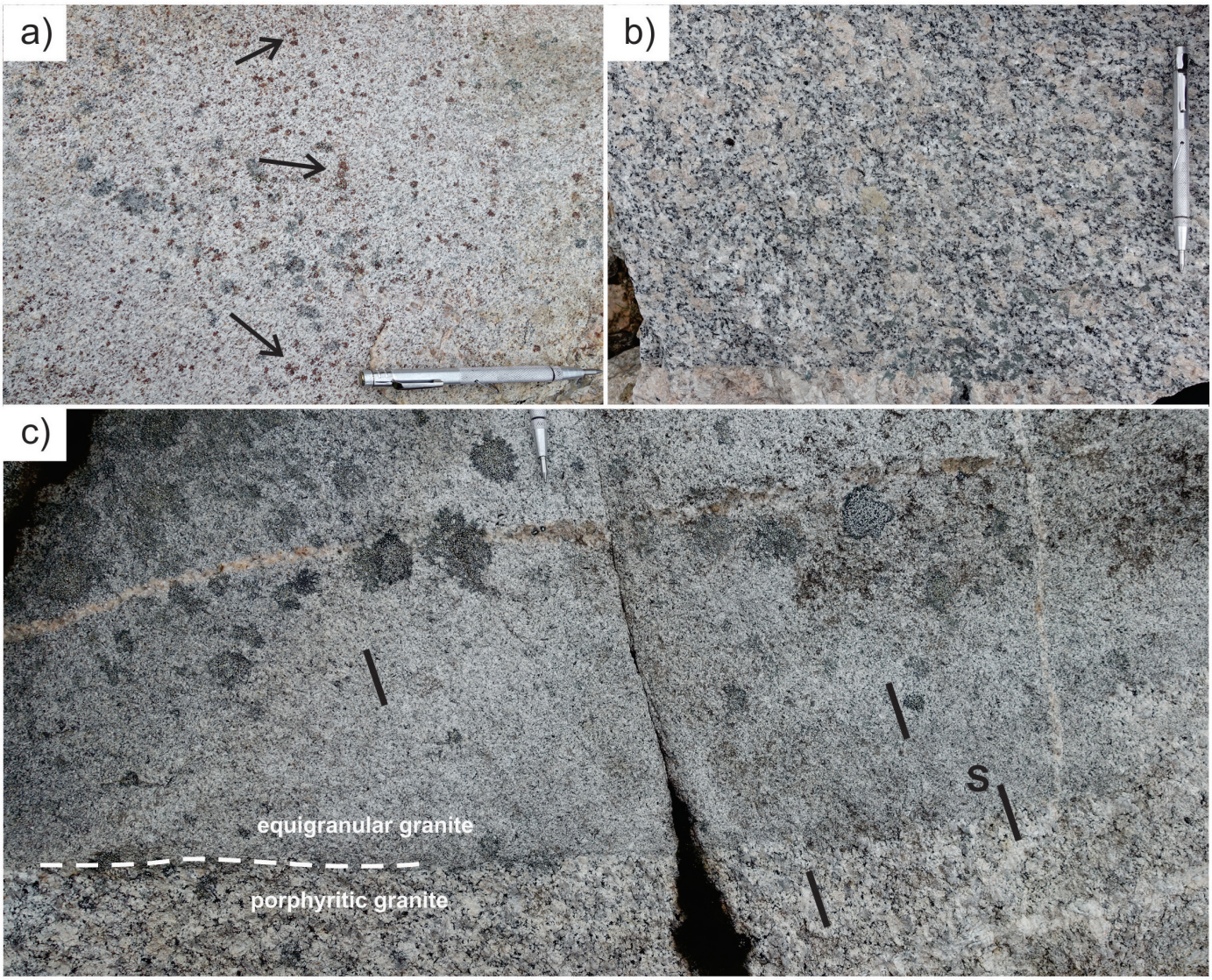

Fig. 9. Representative outcrop photographs of the Mesilinka suite**. a)** Equigranular granite, with red garnet (arrows). **b)** Porphyritic granite with K-feldspar phenocrysts. **c)** Intrusive contact where the porphyritic granite crosscuts the equigranular granite. The contact is cut by the foliation (S), demonstrating this fabric is tectonic, not magmatic.

5. Conclusions

New mapping has refined the subdivision and distribution of plutonic rocks in northern Hogem batholith. The eastern part of the study area is mostly underlain by diorite and lesser hornblendite of the Thane Creek suite. Quartz monzonite also occurs in the Thane Creek suite and may have formed as a result of magmatic differentiation, post-crystallization alteration processes, or both. The diorites consistently have a weak to strong foliation, with local mylonite. Tonalite and granodiorite to quartz monzonite are included in the Thane Creek suite, but appear to post-date the hornblendite and diorite intrusions. Syenite and monzonite, with local monzodiorite and biotite pyroxenite, underlie the southern part of the study area and are part of the Duckling Creek suite. Intrusive contacts with the Thane Creek diorites were not observed, but correlation with dated rocks to the south and north (Schiarizza and Tan, 2005b; Devine et al., 2014), suggests the Thane Creek suite is older (≥ 200 Ma) than the Duckling Creek suite (182 to 175 Ma).

The western part of the study area is underlain by granitic rocks of the Mesilinka suite. All Mesilinka suite rocks are deformed, with foliations that crosscut intrusive contacts. The youngest rocks are in the central part of the study area and consist of Osilinka suite granites, which contain low abundances of mafic minerals (≤5%). These granites lack a foliation, but display local evidence of post-crystallization ductile strain. The Osilinka granite is intruded by subhorizontal sheets and lesser dikes of intermediate feldspar porphyry and felsic quartz-feldspar porphyry, which are the youngest rocks in the study area.

Seventeen new mineral occurrences were discovered during mapping. These are mostly disseminated chalcopyrite and/or malachite staining in rocks of the Thane Creek and Duckling Creek suites, but also include quartz veins that crosscut the Thane Creek and Osilinka suites.

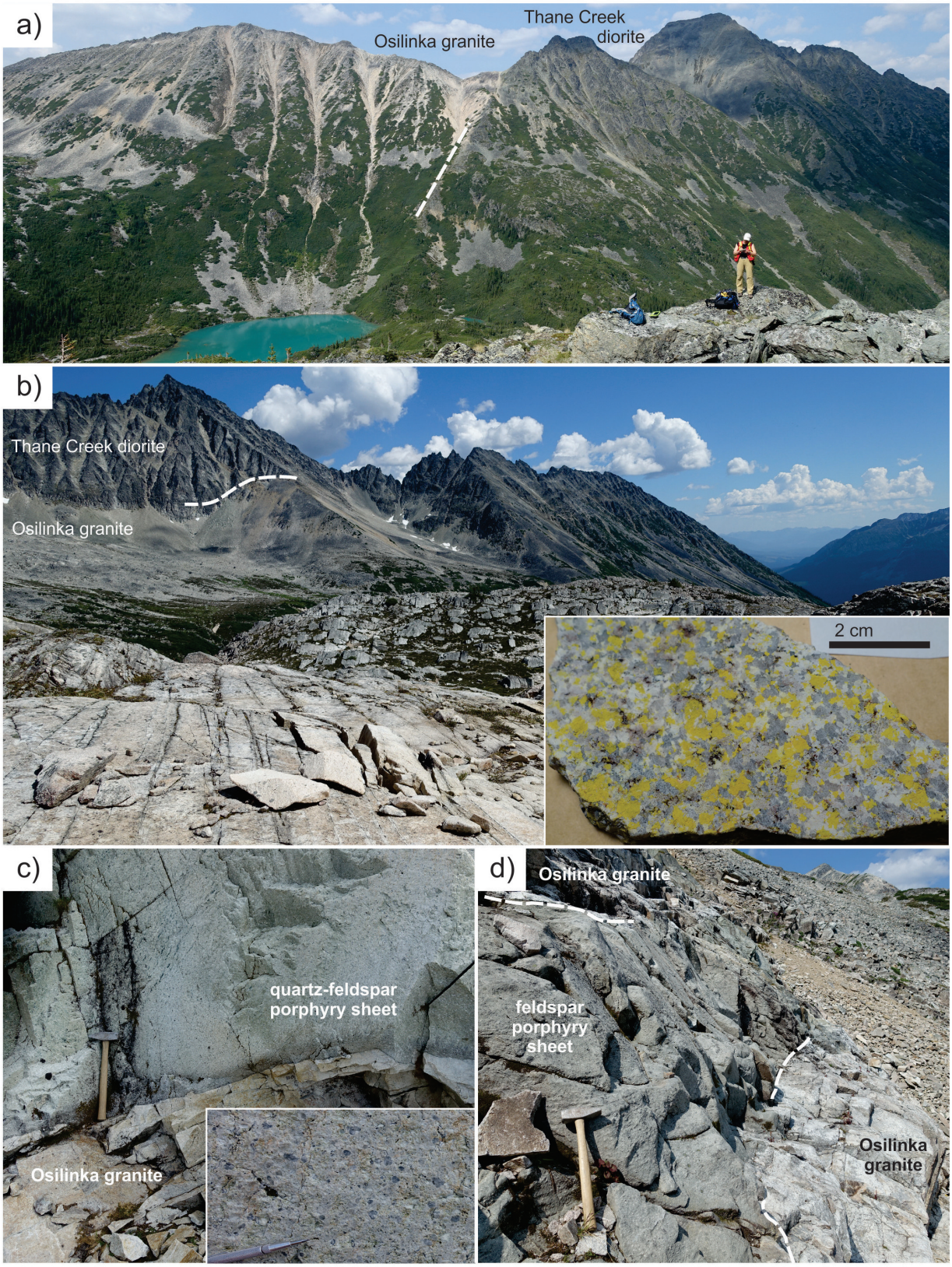

Fig. 10. Osilinka suite and porphyry sheets. **a)** Intrusive contact between the Osilinka granite and Thane Creek diorite. View is north. **b)** Foreground is Osilinka granite with joints (grey fractures) and background is intrusive contact with Thane Creek diorite. View is to the east. Inset is stained Oslinka granite showing K-feldspar (yellow) with quartz (grey), plagioclase (white) and low mafic mineral content. **c)** Subhorizontal quartz-feldspar porphyry sheet that cuts Osilinka granite. Inset shows quartz (blue-grey) and K-feldspar (white) phenocrysts in fine-grained groundmass. **d)** Subhorizontal intermediate feldspar porphyry sheet that cuts Osilinka granite.

Table 2. Mineral occurrences in the study area, extracted and modified from British Columbia Geological Survey MINFILE (https://www2.gov.bc.ca/gov/content/industry/mineral-exploration-mining/british-columbia-geological-survey/mineralinventory).

Label	MINFILE	Name	Alias	Commodities	Deposit type	Status	UTM_X*	UTM_Y*
1	094C 045	HORNWAY CREEK	COPPER 1	Cu	Alkalic porphyry	Showing	321347	6233527
2	094C 098	PAUL	MANIE	Mo	Porphyry	Showing	323755	6232095
3	094C 011	OS		Cu	Alkalic porphyry	Showing	325250	6228567
4	094C 010	ET	CATHEDRAL	Cu	Alkalic porphyry	Showing	326898	6234722
5	094C 016	CHIEF THOMAS	THANE CREEK	Cu	Polymetallic veins	Showing	330105	6232117
6	094C 046	ETSCHITKA CREEK	COPPER 2	Cu	Alkalic porphyry	Showing	330433	6236901
7	094C 047	MATETLO CREEK	COPPER 3	Cu	Alkalic porphyry	Showing	332209	6235593
8	094C 017	ELIZABETH		Au, Ag	Au-quartz veins	Showing	331901	6233903
9	094C 117	YETI		Cu	Alkalic porphyry	Showing	335263	6235227
10	094C 116	BILL	MATE	Cu, Au	Alkalic porphyry	Showing	335190	6233341
11	094C 115	INTREPID	MATE	Cu	Alkalic porphyry	Showing	335473	6232619
12	094C 188	LAKE AREA (CATHEDRAL)	SADDLE	Cu	Alkalic porphyry	Showing	335374	6231511
13	094C 018	MATETLO	KAM	Cu	Alkalic porphyry	Prospect	337907	6232216
14	094C 114	KOALA	MATE	Cu	Alkalic porphyry	Showing	338408	6232692
15	094C 113	YAK	MATE	Cu	Alkalic porphyry	Showing	338744	6232463
16	094C 118	DRAGON	MATE	Cu, Au	Alkalic porphyry	Showing	339143	6233438
17	094C 099	MAT 1	ROLLY	Ag, Cu, Pb, Zn, Au	Polymetallic veins	Prospect	340305	6235468
18	094C 119	TOUGH		Cu	Alkalic porphyry	Showing	343949	6236138
19	094C 174	OSI		Cu, Pt	Alkalic porphyry	Showing	333708	6221450
20	094C 050	HOGEM COPPER	OSILINKA RIVER	Cu	Porphyry	Showing	331784	6221249
21	094C 051	DETNI CREEK	OMINECA RIVER	Cu	Porphyry	Showing	320429	6212794
22	094C 140	HAWK (HSW)	HSW	Au, Cu	Au-quartz veins	Showing	331457	6212471
23	094C 138	HAWK (AD)	AD	Au, Cu, Pb, Zn, Ag	Au-quartz veins	Prospect	333410	6213231
24	094C 171	MEADOW	HAWK	Au, Ag, Cu	Au-quartz veins	Showing	334000	6212160
25	094C 139	HAWK (RADIO)	RADIO	Au, Cu, Ag	Au-quartz veins	Prospect	333702	6211827
26	094C 063	DOVE	HAW	Cu, Mo, Ag	Alkalic porphyry	Showing	331505	6209715
27	093N 171	HAW	HAWK	Cu	Alkalic porphyry	Showing	331533	6207331
28	093N 249	RAVEN		Au, Cu	Alkalic porphyry	Showing	333846	6206636
29	093N 176	FLAME	OGK	Cu, Mo	Alkalic porphyry	Showing	338000	6209032
30	093N 242	SLIDE	JAN-TAM-MISTY	Cu, Au, Ag	Alkalic porphyry	Prospect	341833	6208350
31	094C 097	REM	AMP	Cu, Pb	Polymetallic veins	Showing	345701	6211009
32	094C 077	ND		Cu	Alkalic porphyry	Showing	342102	6210706
33	094C 170	GOAT	TAM	Cu, Au, Ag	Alkalic porphyry	Showing	338429	6211090
34	094C 177	NOVA 5	CAT MOUNTAIN	Cu	Alkalic porphyry	Showing	339595	6214332

Label numbers correspond to Figure 11.

*UTM Zone 10, NAD 83

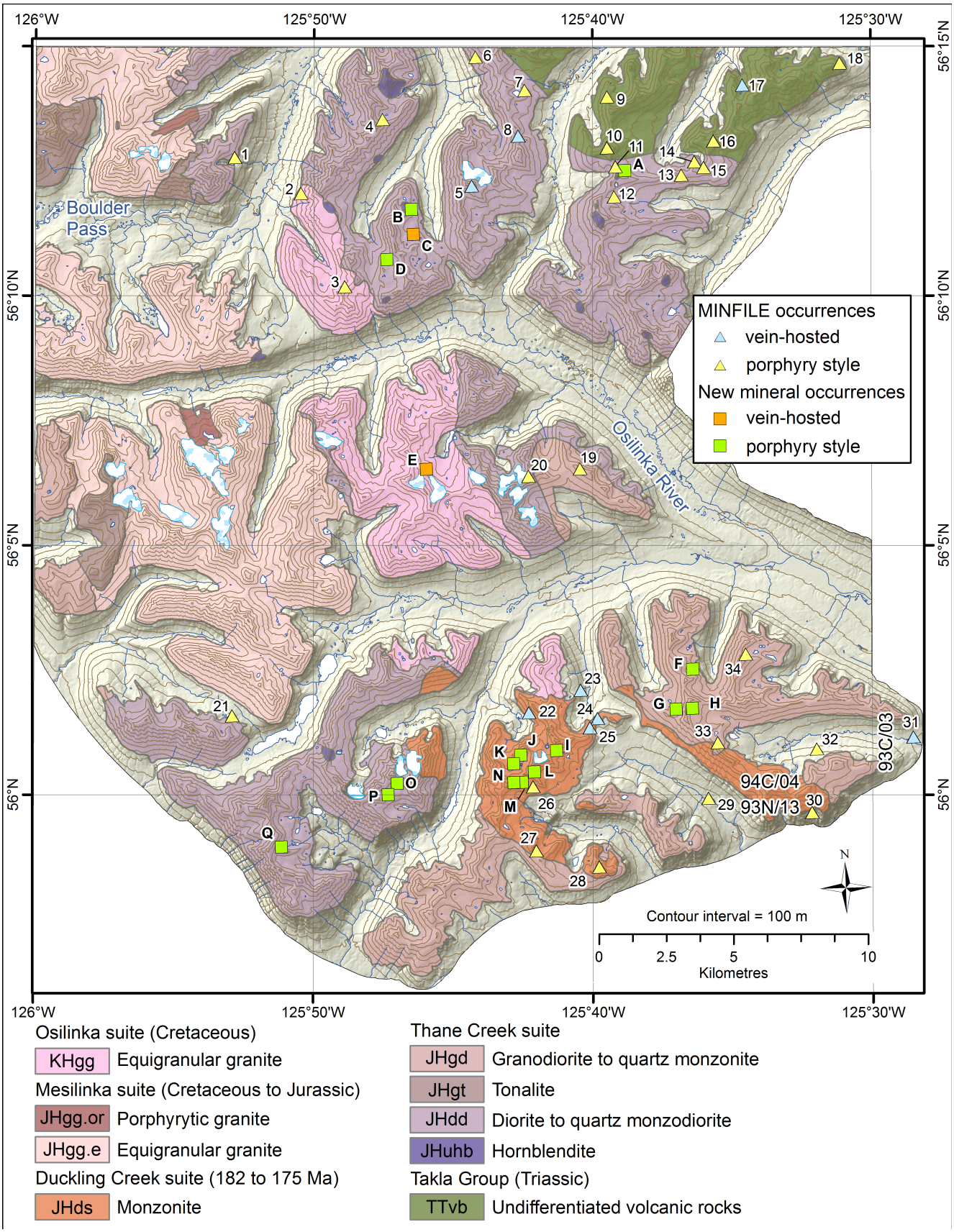

Fig. 11. Mineral occurrences in the study area. MINFILE occurrences are designated by numbers (see Table 2); newly mapped occurrences are designated by letters (see Table 3).

Table 3. Assay results from newly mapped mineral occurrences. Labels correspond to locations plotted on Figure 11; underlined values are considered of interest; *UTM zone 10, NAD 83; ^close to mineralization documented in MINFILE; **may contain lepidolite.

Label		**A**	**B**	**C**	**D**	**E**	**E**	**E**	**F**	**G**
station		18ab-6-3c	18lo-6-2a	18lo-7-2a	18DMI-8-10	18lo-15-1b-1	18lo-15-1b-2	18lo-15-1b-3	18bg-31-1b	18ab-26-4
		^Known	New	New	New	New	New	New	New	New
MINFILE		094C 115								
Type		porphyry	porphyry	vein	porphyry	vein	vein	vein	porphyry	porphyry
UTM_X*		335800	327819	327857	326835	327996	327996	327996	337594	336915
UTM_Y*		6232472	6231338	6230407	6229511	6221663	6221663	6221663	6213838	6212379
Au	ppb	478	46	41	10	1600	3680	612	54	227
Ag	ppm	4.2	1.9	10.3	3.3	2.5	1.1	1.2	1.7	140
Cu	ppm	4430	3170	> 10000	3860	12	10	5	5290	4340
Cu	%	-	-	1.28	-	-	-	-	-	-
Cd	ppm	< 0.3	0.6	1.3	0.5	< 0.3	< 0.3	< 0.3	< 0.3	3.4
Mo	ppm	3	< 1	1	< 1	74	58	65	< 1	32
Pb	ppm	11	< 3	< 3	4	13	6	< 3	< 3	480
Ni	ppm	18	31	8	11	2	4	3	9	3
Zn	ppm	63	115	43	79	10	13	7	43	387
S	%	0.02	3.96	0.75	0.19	5.45	4.49	4.19	0.11	0.44
Al	%	8.07	7.85	1.78	5.89	1.25	3.75	2.02	7.97	7.2
As	ppm	4.9	9.3	2.2	3	1.3	1.6	2.3	2	11.1
Ba	ppm	820	390	500	1050	390	660	550	1700	1680
Be	ppm	1	< 1	< 1	< 1	1	4	2	1	1
Bi	ppm	< 2	< 2	11	< 2	325	106	29	< 2	< 2
Br	ppm	< 0.5	< 0.5	< 0.5	< 0.5	< 0.5	< 0.5	< 0.5	< 0.5	< 0.5
Ca	%	3.03	3.91	0.4	1.73	0.32	0.33	0.66	3.39	1.1
Co	ppm	22	51	11	21	7	8	5	19	10
Cr	ppm	4	31	104	4	3	91	< 2	< 2	40
Cs	ppm	< 1	< 1	< 1	< 1	1	3	2	< 1	< 1
Eu	ppm	1.2	0.6	1.1	0.3	< 0.2	< 0.2	< 0.2	0.5	< 0.2
Fe	%	6.77	11.7	3.21	4.24	5.02	4.58	4.27	3.91	2.93
Hf	ppm	13	< 1	< 1	< 1	< 1	< 1	< 1	4	3
Hg	ppm	< 1	< 1	< 1	< 1	< 1	< 1	< 1	< 1	< 1
Ir	ppb	< 5	< 5	< 5	< 5	< 5	< 5	< 5	< 5	< 5
K	%	3.63	0.28	0.5	1.25	0.8	1.78	1.34	2.31	4.69
Li	ppm	11	6	4	12	4	7	6	9	7
Mg	%	1.5	3.38	0.6	1.4	0.05	0.11	0.07	1.07	0.44
Mn	ppm	897	978	545	775	115	254	138	768	380
Na	%	1.92	2.31	0.1	1.86	0.04	0.31	0.05	2.86	2.02
P	%	0.189	0.266	0.03	0.096	0.001	0.004	0.001	0.101	0.04
Rb	ppm	72	< 15	< 15	< 15	35	115	93	69	128
Sb	ppm	1.4	0.3	0.3	1	< 0.1	< 0.1	< 0.1	0.4	192
Sc	ppm	15.7	24.7	2.7	9.9	0.6	0.8	0.8	9.2	2.5
Se	ppm	< 3	< 3	< 3	< 3	< 3	< 3	< 3	< 3	< 3
Sr	ppm	508	388	29	289	27	56	46	762	101
Ta	ppm	< 0.5	< 0.5	< 0.5	< 0.5	< 0.5	< 0.5	< 0.5	< 0.5	< 0.5
Ti	%	0.18	0.44	0.07	0.23	0.01	0.03	0.02	0.26	0.14
Th	ppm	4	< 0.2	1.5	< 0.2	0.2	0.3	< 0.2	3.5	6.6
U	ppm	11.5	< 0.5	< 0.5	< 0.5	< 0.5	< 0.5	< 0.5	2.8	5.1
V	ppm	66	206	62	102	49	59	66	114	61
W	ppm	< 1	< 1	2	< 1	13	61	164	< 1	16
Y	ppm	26	14	5	9	< 1	< 1	< 1	11	4
La	ppm	20.1	6.2	21	5.3	0.7	0.8	< 0.5	14.6	11.6
Ce	ppm	48	14	40	14	< 3	< 3	< 3	22	17
Nd	ppm	17	15	17	< 5	< 5	< 5	< 5	10	< 5
Sm	ppm	3.7	2.7	4	1.5	< 0.1	< 0.1	0.1	2.5	1
Sn	%	< 0.02	< 0.02	< 0.02	< 0.02	< 0.02	< 0.02	< 0.02	< 0.02	< 0.02
Tb	ppm	< 0.5	< 0.5	< 0.5	< 0.5	< 0.5	< 0.5	< 0.5	< 0.5	< 0.5
Yb	ppm	2.2	1.4	0.5	0.9	< 0.2	< 0.2	< 0.2	1.1	0.5
Lu	ppm	0.26	0.05	0.05	< 0.05	< 0.05	< 0.05	< 0.05	0.1	< 0.05
Mass	g	34.7	34.8	32	33.7	32.2	32.5	32.9	30	31

Table 3. Continued.

Label		**H****	**I**	**J**	**K**	**L**	M	**N**	**O**	**P**
station		18ab-24-11	18lo-24-5a	18ab-17-2	18ab-18-10b	18lo-25-2c	18bg-28-2	18ab-16-9	18ab-23-8	18ab-22-7
MINFILE		New	New	New	New	New	^Known 094C 063	New	New	New
Type		porphyry	porphyry	porphyry	porphyry	porphyry	porphyry	porphyry	porphyry	porphyry
UTM_X*		337530	332420	331080	330806	331567	331098	330783	326452	326100
UTM_Y*		6212386	6211021	6210906	6210596	6210259	6209887	6209894	6210031	6209630
Au	ppb	774	72	73	466	718	300	186	58	119
Ag	ppm	7.8	1.7	1.8	4.3	3.1	5.7	2.1	3.3	9.2
Cu	ppm	19	1910	2150	5660	> 10000	6800	2620	3610	3720
Cu	%	-	-	-	-	1.53	-	-	-	-
Cd	ppm	2.7	< 0.3	< 0.3	0.5	1.1	0.6	< 0.3	0.4	< 0.3
Mo	ppm	2	< 1	< 1	< 1	2	< 1	< 1	5	1
Pb	ppm	149	4	6	8	9	6	< 3	5	22
Ni	ppm	6	5	5	8	26	11	15	9	3
Zn	ppm	285	102	75	69	216	129	193	106	7
S	%	1.42	0.02	0.01	0.17	0.94	0.04	0.06	0.21	0.24
Al	%	7.97	10.1	9.48	8.96	7.59	3.78	4.88	9.19	0.25
As	ppm	2.3	2.5	1.8	< 0.5	1.1	2	2.3	1	1.9
Ba	ppm	940	1740	3130	3310	2600	730	1120	1080	200
Be	ppm	1	2	1	< 1	< 1	3	2	1	< 1
Bi	ppm	< 2	< 2	< 2	< 2	< 2	6	< 2	< 2	17
Br	ppm	< 0.5	< 0.5	< 0.5	< 0.5	< 0.5	< 0.5	< 0.5	< 0.5	< 0.5
Ca	%	4.98	1.78	2.44	3.42	1.17	13.7	9.34	3.18	0.06
Co	ppm	14	14	19	14	60	43	53	37	4
Cr	ppm	40	3	8	23	24	26	31	6	< 2
Cs	ppm	< 1	< 1	< 1	< 1	< 1	< 1	< 1	2	< 1
Eu	ppm	0.4	< 0.2	< 0.2	< 0.2	0.4	3.2	2.8	< 0.2	< 0.2
Fe	%	3.27	3.56	4.14	3.79	8.03	7.49	12.9	5.56	1.41
Hf	ppm	3	4	3	1	2	2	4	4	< 1
Hg	ppm	< 1	< 1	< 1	< 1	< 1	< 1	< 1	< 1	< 1
Ir	ppb	< 5	< 5	< 5	< 5	< 5	< 5	< 5	< 5	< 5
K	%	4.47	6.19	5.96	4.64	5.79	1.43	1.55	1.76	0.04
Li	ppm	5	9	7	2	8	11	14	12	< 1
Mg	%	0.29	0.63	0.66	0.76	1.35	3.71	3.33	1.66	0.03
Mn	ppm	1060	1130	916	924	1240	2930	2780	956	63
Na	%	0.17	2.34	2.15	2.71	1.54	1.19	1.72	3.4	0.12
P	%	0.102	0.074	0.074	0.12	0.264	1.52	0.327	0.096	0.008
Rb	ppm	199	110	149	88	185	< 15	34	< 15	< 15
Sb	ppm	2.4	< 0.1	0.2	< 0.1	< 0.1	< 0.1	< 0.1	< 0.1	< 0.1
Sc	ppm	6.7	4.6	5.7	5.6	2.6	30.8	27.6	10.9	< 0.1
Se	ppm	< 3	< 3	< 3	< 3	< 3	< 3	< 3	< 3	10
Sr	ppm	105	1900	4160	3920	1230	708	990	659	12
Ta	ppm	< 0.5	< 0.5	< 0.5	< 0.5	< 0.5	< 0.5	< 0.5	< 0.5	< 0.5
Ti	%	0.26	0.24	0.19	0.25	0.33	0.02	0.26	0.39	0.01
Th	ppm	3.2	4	2.1	1.8	3.7	6	2.2	1.3	< 0.2
U	ppm	3.8	0.9	< 0.5	< 0.5	1.7	< 0.5	1	< 0.5	< 0.5
V	ppm	108	155	120	192	295	324	317	147	8
W	ppm	34	< 1	< 1	< 1	< 1	< 1	< 1	< 1	< 1
Y	ppm	8	8	11	13	13	60	38	10	< 1
La	ppm	13.7	8.4	8.2	13.9	16.5	100	33.5	12.6	1.3
Ce	ppm	23	17	18	29	29	151	63	18	< 3
Nd	ppm	11	< 5	9	8	11	50	23	8	< 5
Sm	ppm	2.2	1.5	2.3	2.8	2.5	12	7.7	1.7	< 0.1
Sn	%	< 0.02	< 0.02	< 0.02	< 0.02	< 0.02	< 0.02	< 0.02	< 0.02	< 0.02
Tb	ppm	< 0.5	< 0.5	< 0.5	< 0.5	< 0.5	2.1	1.4	< 0.5	< 0.5
Yb	ppm	0.9	0.9	1.1	1.1	1	4.4	3.2	1	< 0.2
Lu	ppm	0.1	< 0.05	0.07	0.07	0.07	0.28	0.15	< 0.05	< 0.05
Mass	g	30	37.4	34.7	30.2	33.1	38.3	37.3	32.4	36.7

Table 3. Continued.

Label		Q								
station		18bg-26-2b	18ab-23-7	18ab-26-9	18ab-6-3a	18bg-19-2	18bg-25-2b	18bg-25-7	18bg-27-7	18bg-29-8a
		New								
MINFILE										
Type		porphyry								
UTM_X*		322055	326536	336101	335800	324553	322661	321909	338051	329741
UTM_Y*		6207840	6209997	6212567	6232472	6220350	6208033	6209181	6212345	6206600
Au	ppb	232	7	27	< 2	6	7	2	249	< 2
Ag	ppm	5.8	0.3	0.8	0.4	4	0.4	< 0.3	1.5	< 0.3
Cu	ppm	3580	716	11	178	114	86	21	43	238
Cu	%	-	-	-	-	-	-	-	-	-
Cd	ppm	0.4	< 0.3	< 0.3	< 0.3	< 0.3	< 0.3	< 0.3	0.5	< 0.3
Mo	ppm	1	4	21	< 1	9	2	< 1	3	< 1
Pb	ppm	14	< 3	16	< 3	1200	< 3	< 3	16	< 3
Ni	ppm	6	3	5	16	4	5	2	3	8
Zn	ppm	12	5	6	54	13	21	5	15	62
S	%	0.41	0.02	0.03	0.1	0.25	0.44	0.03	0.21	0.04
Al	%	1.55	1	0.65	7.14	4.63	2.86	0.24	4.05	8.71
As	ppm	5.1	2.6	2.1	2.5	4.3	1.5	3	1.5	< 0.5
Ba	ppm	< 50	< 50	240	610	2810	790	930	740	2120
Be	ppm	< 1	< 1	< 1	1	2	< 1	< 1	< 1	1
Bi	ppm	< 2	< 2	< 2	< 2	11	< 2	< 2	< 2	< 2
Br	ppm	< 0.5	< 0.5	< 0.5	< 0.5	< 0.5	< 0.5	< 0.5	< 0.5	< 0.5
Ca	%	0.32	1.32	0.46	7	0.49	0.28	0.5	0.14	2.29
Co	ppm	9	2	2	21	< 1	15	< 1	5	14
Cr	ppm	119	124	162	26	< 2	3	< 2	85	28
Cs	ppm	< 1	< 1	< 1	6	< 1	< 1	< 1	< 1	< 1
Eu	ppm	< 0.2	< 0.2	< 0.2	1.1	< 0.2	< 0.2	< 0.2	< 0.2	< 0.2
Fe	%	2.06	1.27	0.62	7.59	0.74	2.38	0.51	1.23	3.73
Hf	ppm	< 1	< 1	< 1	30	1	< 1	< 1	< 1	4
Hg	ppm	< 1	< 1	< 1	< 1	< 1	< 1	< 1	< 1	< 1
Ir	ppb	< 5	< 5	< 5	< 5	< 5	< 5	< 5	< 5	< 5
K	%	0.07	0.03	0.59	2.05	1.03	0.98	0.06	4.36	2.47
Li	ppm	< 1	< 1	3	6	16	3	< 1	2	15
Mg	%	0.1	< 0.01	0.05	0.74	0.06	0.38	0.03	0.02	1.26
Mn	ppm	161	248	270	1120	238	416	158	169	797
Na	%	1.01	0.03	0.06	2.05	2.25	0.36	0.12	0.15	2.97
P	%	0.009	0.005	0.005	0.255	0.008	0.035	0.003	0.02	0.108
Rb	ppm	< 15	< 15	< 15	60	< 15	26	< 15	109	98
Sb	ppm	0.3	0.2	2	2.4	0.2	< 0.1	< 0.1	0.3	0.1
Sc	ppm	3	0.8	0.3	33.7	1.3	6.1	0.2	1.6	8.9
Se	ppm	< 3	< 3	< 3	< 3	< 3	< 3	< 3	< 3	< 3
Sr	ppm	50	201	45	144	889	43	66	70	510
Ta	ppm	< 0.5	< 0.5	< 0.5	< 0.5	< 0.5	< 0.5	< 0.5	< 0.5	< 0.5
Ti	%	0.08	0.02	0.02	0.43	0.04	0.14	0.01	0.09	0.28
Th	ppm	< 0.2	< 0.2	0.2	1.6	< 0.2	< 0.2	1.5	2.3	4.8
U	ppm	< 0.5	< 0.5	0.6	1.5	< 0.5	0.6	< 0.5	< 0.5	2.7
V	ppm	65	46	5	254	21	99	4	21	115
W	ppm	< 1	< 1	< 1	8	8	15	< 1	16	< 1
Y	ppm	2	1	2	24	2	3	< 1	2	12
La	ppm	1.2	0.6	2	17.9	1.4	2	3.5	7.7	13.4
Ce	ppm	< 3	< 3	3	45	< 3	4	6	12	20
Nd	ppm	< 5	< 5	< 5	8	< 5	< 5	< 5	< 5	9
Sm	ppm	0.1	< 0.1	0.3	4.4	0.2	0.3	0.2	0.8	2.4
Sn	%	< 0.02	< 0.02	< 0.02	< 0.02	< 0.02	0.03	< 0.02	< 0.02	< 0.02
Tb	ppm	< 0.5	< 0.5	< 0.5	< 0.5	< 0.5	< 0.5	< 0.5	< 0.5	< 0.5
Yb	ppm	< 0.2	< 0.2	< 0.2	3	< 0.2	0.4	< 0.2	0.3	1.4
Lu	ppm	< 0.05	< 0.05	< 0.05	0.24	< 0.05	< 0.05	< 0.05	< 0.05	0.1
Mass	g	33.1	32.8	32.4	32.3	31.7	34.4	33.9	30.3	30.6

Table 3. Continued.

Label station		18DMI-6-5c	18DMI-8-9	18lo-10-1c	18 lo-11-4	18lo-16-3	18lo-18-6	18lo-19-3e	18lo-3-3	18lo-4-3
MINFILE										
Type										
UTM_X*		326795	326970	327036	318473	328230	329386	327259	327818	328406
UTM_Y*		6229078	6229561	6235679	6234670	6222501	6219042	6210680	6230415	6229794
Au	ppb	< 2	4	5	< 2	7	37	11	18	8
Ag	ppm	< 0.3	< 0.3	3.4	< 0.3	< 0.3	0.8	< 0.3	< 0.3	< 0.3
Cu	ppm	2	67	725	18	11	441	25	75	87
Cu	%	-	-	-	-	-	-	-	-	-
Cd	ppm	< 0.3	< 0.3	< 0.3	< 0.3	< 0.3	< 0.3	< 0.3	< 0.3	< 0.3
Mo	ppm	< 1	24	7	1	19	5	< 1	< 1	19
Pb	ppm	< 3	< 3	< 3	< 3	< 3	3	25	< 3	< 3
Ni	ppm	5	4	6	4	3	5	4	6	8
Zn	ppm	10	2	15	2	3	21	140	25	52
S	%	< 0.01	0.18	0.2	0.29	0.94	1.75	0.33	0.42	0.21
Al	%	0.27	0.51	5.46	0.78	2.4	0.2	7.39	1.1	7.77
As	ppm	< 0.5	< 0.5	3.5	2.4	1.1	6.6	1.5	1.4	3.8
Ba	ppm	< 50	70	1120	230	510	< 50	1720	220	210
Be	ppm	< 1	< 1	< 1	< 1	1	< 1	< 1	< 1	< 1
Bi	ppm	< 2	< 2	31	< 2	13	12	< 2	< 2	< 2
Br	ppm	< 0.5	< 0.5	< 0.5	< 0.5	< 0.5	< 0.5	< 0.5	< 0.5	< 0.5
Ca	%	0.24	0.32	1.7	0.05	0.03	< 0.01	2.85	0.39	7.68
Co	ppm	2	4	51	2	< 1	5	12	14	13
Cr	ppm	8	124	87	112	105	87	< 2	116	5
Cs	ppm	< 1	< 1	2	1	2	< 1	2	< 1	< 1
Eu	ppm	< 0.2	< 0.2	< 0.2	< 0.2	< 0.2	1	< 0.2	< 0.2	0.9
Fe	%	0.67	1.75	2.68	0.8	2.63	8.83	3.05	2.26	6.83
Hf	ppm	< 1	< 1	< 1	< 1	< 1	< 1	4	< 1	< 1
Hg	ppm	< 1	< 1	< 1	< 1	< 1	< 1	< 1	< 1	< 1
Ir	ppb	< 5	< 5	< 5	< 5	< 5	< 5	< 5	< 5	< 5
K	%	< 0.01	0.08	1.48	0.54	1.41	0.06	2.58	0.16	0.24
Li	ppm	2	< 1	3	5	3	1	7	4	5
Mg	%	0.24	0.02	0.35	0.01	0.02	< 0.01	0.83	0.54	1.29
Mn	ppm	152	96	215	59	115	18000	1050	390	1070
Na	%	0.02	0.15	0.74	0.17	0.5	0.02	2.73	0.12	1.88
P	%	0.001	0.007	0.172	0.004	0.003	0.002	0.077	0.013	0.121
Rb	ppm	< 15	< 15	< 15	< 15	81	< 15	30	< 15	< 15
Sb	ppm	0.1	0.3	< 0.1	0.4	0.1	0.1	0.4	0.2	1.1
Sc	ppm	0.9	1.1	2.2	0.4	0.5	0.2	5.4	1.5	12
Se	ppm	< 3	< 3	< 3	< 3	< 3	< 3	< 3	< 3	< 3
Sr	ppm	6	97	300	33	50	21	457	28	1470
Ta	ppm	< 0.5	< 0.5	< 0.5	< 0.5	< 0.5	< 0.5	< 0.5	< 0.5	< 0.5
Ti	%	< 0.01	0.02	0.07	0.06	0.01	< 0.01	0.23	0.04	0.34
Th	ppm	< 0.2	< 0.2	< 0.2	0.6	< 0.2	< 0.2	1.1	0.3	1
U	ppm	< 0.5	< 0.5	< 0.5	1.4	< 0.5	< 0.5	< 0.5	< 0.5	0.9
V	ppm	16	21	53	4	8	< 2	86	31	228
W	ppm	< 1	< 1	1	4	4	72	7	< 1	< 1
Y	ppm	< 1	< 1	3	1	< 1	4	4	2	9
La	ppm	< 0.5	0.5	4.7	0.9	< 0.5	8.3	7.6	2.6	8.8
Ce	ppm	< 3	< 3	7	< 3	< 3	12	12	5	15
Nd	ppm	< 5	< 5	< 5	< 5	< 5	< 5	< 5	< 5	7
Sm	ppm	< 0.1	0.1	1	< 0.1	< 0.1	0.6	1	0.5	1.8
Sn	%	< 0.02	< 0.02	< 0.02	< 0.02	< 0.02	< 0.02	0.04	< 0.02	< 0.02
Tb	ppm	< 0.5	< 0.5	< 0.5	< 0.5	< 0.5	< 0.5	< 0.5	< 0.5	< 0.5
Yb	ppm	< 0.2	< 0.2	< 0.2	< 0.2	< 0.2	0.4	0.7	< 0.2	0.9
Lu	ppm	< 0.05	< 0.05	< 0.05	< 0.05	< 0.05	< 0.05	< 0.05	< 0.05	< 0.05
Mass	g	36.4	34.8	31.7	32.6	31.3	31.5	31.7	32.9	35.3

Table 3. Continued.

Label station		18lo-5-5	18lo-5-5b	18lo-6-2c	18lo-7-2b	18ab-24-2	Analysis Method	Detection Limit
MINFILE Type								
UTM_X*		330919	330919	327819	327857	337895		
UTM_Y*		6233783	6233783	6231338	6230407	6211421		
Au	ppb	15	11	< 2	13	< 2	INAA	2
Ag	ppm	0.5	0.7	< 0.3	0.8	< 0.3	MULT INAA / TD-ICP	0.3
Cu	ppm	45	46	397	288	16	TD-ICP	1
Cu	%	-	-	-	-	-	4Acid ICPOES	0.001
Cd	ppm	< 0.3	< 0.3	< 0.3	< 0.3	< 0.3	TD-ICP	0.3
Mo	ppm	5	4	< 1	2	< 1	TD-ICP	1
Pb	ppm	72	112	4	< 3	< 3	TD-ICP	3
Ni	ppm	3	4	32	5	6	MULT INAA / TD-ICP	1
Zn	ppm	8	7	124	10	7	MULT INAA / TD-ICP	1
S	%	3.53	5.28	0.52	0.1	< 0.01	TD-ICP	0.01
Al	%	1.69	1.91	5.21	0.56	0.95	TD-ICP	0.01
As	ppm	16.4	26.4	2	3.3	< 0.5	INAA	0.5
Ba	ppm	350	390	610	190	180	INAA	50
Be	ppm	< 1	< 1	< 1	< 1	< 1	TD-ICP	1
Bi	ppm	298	480	< 2	< 2	< 2	TD-ICP	2
Br	ppm	< 0.5	< 0.5	< 0.5	< 0.5	< 0.5	INAA	0.5
Ca	%	0.46	0.37	6.49	0.12	0.5	TD-ICP	0.01
Co	ppm	11	9	69	10	3	INAA	1
Cr	ppm	3	4	25	125	148	INAA	2
Cs	ppm	< 1	< 1	6	< 1	< 1	INAA	1
Eu	ppm	< 0.2	< 0.2	1.5	< 0.2	< 0.2	INAA	0.2
Fe	%	5.36	5.41	11.8	1.6	0.86	INAA	0.01
Hf	ppm	< 1	< 1	2	< 1	< 1	INAA	1
Hg	ppm	< 1	< 1	< 1	< 1	< 1	INAA	1
Ir	ppb	< 5	< 5	< 5	< 5	< 5	INAA	5
K	%	0.74	0.87	1.94	0.16	0.23	TD-ICP	0.01
Li	ppm	2	< 1	19	1	6	TD-ICP	1
Mg	%	0.25	0.08	5.58	0.18	0.16	TD-ICP	0.01
Mn	ppm	1500	1130	1230	156	356	TD-ICP	1
Na	%	0.04	0.04	0.49	0.04	0.28	INAA	0.01
P	%	0.027	0.016	0.011	0.006	0.015	TD-ICP	0.001
Rb	ppm	30	33	19	< 15	< 15	INAA	15
Sb	ppm	0.1	0.2	< 0.1	0.3	0.1	INAA	0.1
Sc	ppm	2.7	1.5	55.8	1.1	1.1	INAA	0.1
Se	ppm	< 3	< 3	< 3	< 3	< 3	INAA	3
Sr	ppm	16	12	323	8	101	TD-ICP	1
Ta	ppm	< 0.5	< 0.5	< 0.5	< 0.5	< 0.5	INAA	0.5
Ti	%	0.08	0.06	0.4	0.02	0.05	TD-ICP	0.01
Th	ppm	1	1.7	< 0.2	< 0.2	1.6	INAA	0.2
U	ppm	< 0.5	< 0.5	< 0.5	< 0.5	< 0.5	INAA	0.5
V	ppm	36	25	350	22	15	TD-ICP	2
W	ppm	11	9	< 1	< 1	< 1	INAA	1
Y	ppm	9	2	27	< 1	2	TD-ICP	1
La	ppm	3.7	4.8	5.3	0.6	3.1	INAA	0.5
Ce	ppm	6	7	19	< 3	4	INAA	3
Nd	ppm	< 5	< 5	< 5	< 5	< 5	INAA	5
Sm	ppm	0.7	0.7	4.2	0.2	0.3	INAA	0.1
Sn	%	< 0.02	< 0.02	< 0.02	< 0.02	< 0.02	INAA	0.02
Tb	ppm	< 0.5	< 0.5	< 0.5	< 0.5	< 0.5	INAA	0.5
Yb	ppm	0.8	0.2	2.5	< 0.2	< 0.2	INAA	0.2
Lu	ppm	0.05	< 0.05	0.07	< 0.05	< 0.05	INAA	0.05
Mass	g	33.7	32.8	36.3	31.2	31.1	INAA	

Acknowledgments

Field assistance was from Gaby Jones, Silken Rauhala, and Dylan Spence. A field visit and discussions with Fil Ferri helped improve our understanding of the study area. We thank Silver King helicopters for air support and Cassiar Geoscience for expediting services. Reviews by F. Devine and P. Schiarizza helped improve the clarity of the manuscript.

References cited

Armstrong, J.E., 1946. Aiken Lake (south half), British Columbia. Geological Survey of Canada, Paper 46-11, scale 1 inch:2 miles.

Armstrong, J.E., 1948. Fort St. James, British Columbia. Geological Survey of Canada, A Series Map 907A, scale 1 inch:4 miles.

Armstrong, J.E., and Roots, E.F., 1948. Aiken Lake map-area, British Columbia. Geological Survey of Canada, Paper 48-5, 46 p.

Armstrong, J.E., and Roots, E.F., 1954. Aiken Lake, Cassiar District, British Columbia. Geological Survey of Canada, A Series Map 1030A, scale 1 inch:4 miles.

Bath, A.B., Cooke, D.R., Friedman, R.M., Faure, K., Kamenetsky, V.S., Tosdal, R.M., and Berry, R.F., 2014. Mineralization, U-Pb geochronology, stable isotope geochemistry of the Lower Main Zone of the Lorraine deposit, north-central British Columbia: A replacement-style alkalic Cu-Au porphyry. Economic Geology, 109, 979-1004.

Devine, F.A.M., Chamberlain, C.M., Davies, A.G.S., Friedman, R., and Baxter, P., 2014. Geology and district-scale setting of tilted alkalic porphyry Cu-Au mineralization at the Lorraine deposit, British Columbia. Economic Geology, 109, 939-977.

Ferri, F., Dudka, S.F., Rees, C.J., Meldrum, D.G., and Willson, M.J., 2001. Geology of the Uslika Lake Area, north-central B.C. (NTS 94C/2, 3 & 4). British Columbia Ministry of Energy and Mines, British Columbia Geological Survey Geoscience Map 2001-04, scale 1:50,000.

Garnett, J.A., 1972, Preliminary geological map of part of Hogem batholith, Duckling Creek area (parts of NTS 93N/13, 14; 94C/3, 4). British Columbia Ministry of Energy, Mines and Petroleum Resources, British Columbia Geological Survey Preliminary Map 09.

Garnett, J.A., 1978. Geology and mineral occurrences of the southern Hogem batholith. British Columbia Ministry of Energy, Mines and Petroleum Resources, British Columbia Geological Survey Bulletin 70, 75 p.

Lord, C.S., 1949. McConnell Creek, Cassiar District, British Columbia. Geological Survey of Canada, A Series Map 962A, scale 1 inch:4 miles.

Madu, B.E., and Ballantyne, T., 2018. Search project: Phase III activities in north-central British Columbia (Phase III, covering NTS 094C, D, E, F, 093M, N). Geoscience BC Summary of Activities 2017: Minerals and Mining, Geoscience BC, Report 2018-1, pp. 1-6.

Nelson, J., Carmichael, B., and Gray, M., 2003. Innovative gold targets in the Pinchi Fault/Hogem batholith area: The Hawk and Axelgold properties, central British Columbia (94C/4, 94N/13). In: Geological Fieldwork 2002, British Columbia Ministry of Energy and Mines, British Columbia Geological Survey Paper 2003-1, pp. 97-114.

Nelson, J.L., Colpron, M., and Israel, S., 2013. The Cordillera of British Columbia, Yukon, and Alaska: Tectonics and metallogeny. In: Colpron, M., Bissing, T., Rusk, B.G., and Thompson, J.F.H., (Eds.), Tectonics, Metallogeny, and Discovery: The North American Cordillera and similar accretionary settings. Society of Economic Geologists, Special Publication 17, pp. 53-109.

Nixon, G.T., and Peatfield, G.R., 2003. Geological setting of the Lorraine Cu-Au porphyry deposit, Duckling Creek Syenite Complex, north-central British Columbia. British Columbia Ministry of Energy and Mines, British Columbia Geological Survey Open File 2003-4, 24 p.

Ootes, L., Bergen, A.L., Milidragovic, D., and Graham, B., 2019. Preliminary geology of Notch Peak and Ogden Creek (parts of NTS 094C/04 and 093N/13), northern Hogem batholith, Quesnel terrane, north-central British Columbia. British Columbia Ministry of Energy, Mines and Petroleum Resources, British Columbia Geological Survey Open File 2019-02, scale 1:50,000.

Roots, E.F., 1954. Geology and mineral deposits of Aiken Lake map-area, British Columbia. Geological Survey of Canada, Memoir 274, 246 p.

Schiarizza, P., and Tan, S.H., 2005a. Geology and mineral occurrences of the Quesnel terrane between the Mesilinka River and Wrede Creek (NTS 94D/8, 9), north-central British Columbia. In: Geological Fieldwork 2004, British Columbia Ministry of Energy and Mines, British Columbia Geological Survey Paper 2005-1, pp. 109-130.

Schiarizza, P., and Tan, S.H., 2005b. Geology of the Johanson Lake area, parts of NTS 94D/8 and 9. British Columbia Ministry of Energy and Mines, British Columbia Geological Survey Open File 2005-4; scale 1:50,000.

Woodsworth, G.J., 1976. Plutonic rocks of McConnell Creek (94 D west half) and Aiken Lake (94 C east half) map-areas, British Columbia. Geological Survey of Canada, Paper 76-1A, pp. 69-73.

Woodsworth, G.J., Anderson, R.G., and Armstrong, R.L., 1991. Plutonic regimes, Chapter 15. In: Gabrielse, H., and Yorath, C.J. (Eds.), Geology of the Cordilleran Orogen in Canada, Geological Survey of Canada, Geology of Canada, no. 4, pp. 491-531.